

6 RF Measurements and Characterization of Conductive Textile Materials

by

N. Stathopoulos, S. Savaidis and S. Mitilineos

Department of Electronics Engineering, TEI of Piraeus, Greece

6.1 Introduction

Conductive textile materials have been of great interest during the last decades, mainly due to their applications in the fields of human safety and health monitoring. Most of these applications are related in one way or another with sensor technology, where conductive textile materials are used in a wide range of low-power, low-frequency electronic applications. However, high frequency applications have also been proposed recently, mainly in the field of electrotexile wearable antennas (P.J. Soh, 2011) (Y.J. Ouyang, 2008). Wearable antennas could be useful for applications like life-jackets and RFID passive tags, although they have strong competition from the wearable, flexible metallic structures. Other applications, like electromagnetic shielding, have been successfully applied for the protection of human health from hazardous electromagnetic radiation.

Recently there have been efforts to evaluate the available conductive textile materials as well as to study their properties in high frequencies (D. Cottet, 2003) (Y.J. Ouyang a. W., 2007). It is critical here to recognize all the basic obstacles when using conductive textile materials in high frequencies. Specifically, all high frequency devices are very sensitive to the following properties: -dimensions, -geometry, -conductivity, -symmetry, -dielectric characteristics. Unfortunately, it is difficult for textiles to have inherently the appropriate properties and therefore be suitable for an HF application. On the other hand, how high could the frequency be in order to be used in conductive textiles effectively? Before we answer this question we have to discuss the influence of the frequency range on the operation of a device.

Actually for frequencies right above 1MHz, the influence of parasitic capacitance and the coupling between inductive elements is evident, while these influences become stronger as the frequency increases. Up to a few hundreds of MHz, passive elements like inductors and capacitors are discrete and can be connected to a circuit configuration as individual components. However, all parasitic and couplings should be taken into account, in order to keep the device within its specifications. The use of metallic shields is a very common technique in order to avoid undesired couplings in this range of frequencies. Furthermore, for frequencies higher than 1GHz, the pc-board with its track for component connections, acts as a part of the circuit and its material should have suitable dielectric characteristics in order to keep the device in operation.

Since the RF and microwave (MW) spectrum covers almost all frequencies, from a few hundreds KHz up to hundreds of GHz, the electro-textile materials herein are going to be tested and characterized only for the lower range of the RF spectrum (VHF and UHF range of frequencies). Practically, this will cover frequencies up to 3 GHz which means that the equivalent wavelength will not be less than 10 cm. In this range, the dimensions of textiles in use will be large enough for the tests.

Recently, a thorough work on electrotexile measurements for HF applications has been presented by Ouyang and Chappell (Y.J. Ouyang, 2008). Therein, the materials under test act as coupling components between two high frequency cavities. The shielding properties of conductive textiles are measured through the coupling power from one cavity to the other, while the tests have also been extended to microstrip resonators. A rather similar method has been described and applied within this chapter, but the textile material acts as a resonator itself in conduction with a copper microstrip transmission line. Although an extensive characterization method for textile transmission lines has also presented by Cottet et al. (D. Cottet, 2003), they focus on the transmission lines parameters, rather than a macroscopic study of their ability to conserve electromagnetic energy at a resonance frequency.

On top of the above, textile antennas have been introduced in order to integrate multiple transceiver components on textile substrates for HF frequencies applications and above. Textile antennas may consist of metallic plates over fabric substrate, but recently antennas fabricated with solely textile materials have been also introduced. The development of textile antennas can be traced back to the beginning of the new millennium, when wearable antennas partially based on textiles were first presented. Nowadays, textile antennas are considered a novel technology, but having already come up with certain design examples and constructions in several frequency bands. The respective research field is very active and ongoing research includes new materials and techniques for robustness, durability and credibility of designs.

The scope of this chapter is to present transmission lines and patch antennas layouts for (i) the evaluation of electrotexile materials in HF applications and (ii) the evaluation of electrotexile patch antennas in HF, RF and MW applications. The relative objectives are on the one hand the analysis of T-resonator devices and the experimental setups and measurements, and on the other hand the achieved VSWR, radiation pattern and gain of the antenna respectively. The chapter is organized as follows: In section 6.2, an elementary theory of transmission lines is roughly presented. This section has been considered necessary for the reader, in order to familiarize himself with the basic transmission line terminology. In section 6.3, a thorough presentation of coaxial T resonator and the relative measurements are presented, while in section 6.4 its microstrip version is presented. Section 6.5 includes a short introduction to antenna theory and microstrip antennas in order to familiarize the reader with the respective concepts, while in Section 6.6 early measurements results of textile antennas available in the literature are presented. The chapter concludes with Section 6.7.

SIMPLY CLEVER

ŠKODA



We will turn your CV into
an opportunity of a lifetime



Do you like cars? Would you like to be a part of a successful brand?
We will appreciate and reward both your enthusiasm and talent.
Send us your CV. You will be surprised where it can take you.

Send us your CV on
www.employerforlife.com



6.2 Elementary transmission lines theory

6.2.1 Introduction

A transmission line is a system of conductors that is able to transfer electric power from a source to a load (this definition applies to any frequency range; minimum loss of power over the line is implied but not necessary). A typical application of transmission lines is that of the electric power distribution system where, the energy source is at a low frequency (eg 50 or 60Hz, without excluding the zero frequency). In this case we refer to the transmission of electrical energy produced by large or medium-sized production units, for distribution to residential and industrial consumers.

However, in many other applications, e.g. in telecommunications, the transmission of the electric power is carried out at high frequencies and the source should drive a load (e.g. an antenna) through a transmission line that has the form of a metallic rectangular waveguide i.e. quite different than the two parallel cables of the transmission lines in low frequencies. Moreover, at high frequencies, the transmission lines can be used in applications where their purpose is not to transfer energy from the source to a load. In these cases we exploit the distributed electrical characteristics of lines (distributed inductance and capacitance) to construct passive circuits that can not be constructed using discrete components.

Parallel conductors

Dielectric material

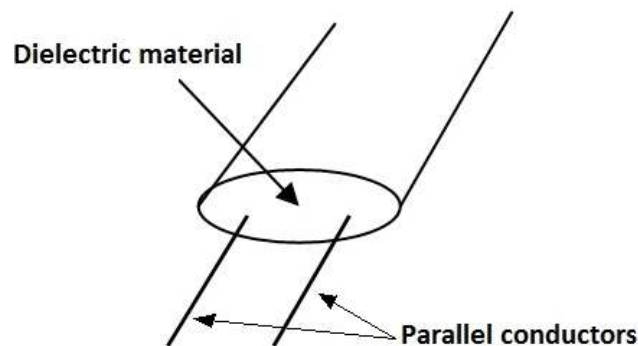


Figure 6.1: A cable of two parallel conductors.

The form of transmission lines used at high frequency applications (i.e. RF and MW), depends mainly on the operating frequency and can be categorized into the following cases:

- Cables with two parallel wires: They consist of two parallel cylindrical conductors at a specific distance between them, bounded by a low loss dielectric material. They have been used in the past for TV applications (receiver-antenna cable) in the VHF frequency range (Figure 6.1).

- Telephone and data transfer lines: These lines consist of twisted pairs of insulated conductors (Figure 6.2). By twisting the conductors we avoid electromagnetic interference and noise effects from the environment and thus support reliable data transmission in local computer networks (like e.g. Ethernet, wherein each cable contains 4 twisted pairs of conductors). The twisted pairs of cables are placed inside an insulating cylindrical shell which may contain an internal metal cover to shield from external interference. These cables are transmission lines capable of carrying high frequency data signals (typically up to 100MHz) at distances of up to 100m.

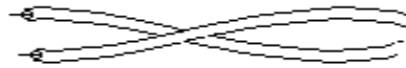


Figure 6.2: Twisted pair telephone cable.

- Coaxial cables for high frequencies: These cables (Figure 6.3) are used in a wide range of applications such as broadcasting of television signals between antenna and receiver, transmission of high-speed data (Ethernet) and many other applications that reach microwave frequencies. The basic type of coaxial cable used in practice is the RG type. For the purposes of Greek domestic TV cable, the RG-58 / U type is commonly used, while for Ethernet applications the RG-8 / U has been used.

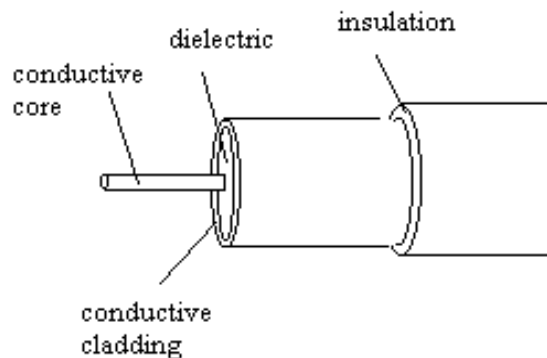


Figure 6.3: Coaxial cable.

- Microstrip lines (Figure 6.4): They are used for the connectivity and implementation of microwave passive networks that are going to be implemented on a pc-board that is made by high frequency, low-loss dielectric materials. With short or open termination, they are used as equivalent inductors or capacitors, while by using their self resonance characteristics they are applied as high frequency resonators. The pc-board dielectric materials are of great importance due to their low losses at high frequencies. For this reason the most common substrate materials in use are mainly Teflon-based.

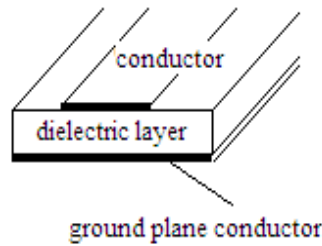


Figure 6.4: Microstrip transmission line.

- Metallic orthogonal waveguides (Figure 6.5): They are used in the microwave range of frequencies and their typical application is for the transfer of power from the high power transmitter to a high power antenna (e.g. a horn antenna). Their use also covers all the applications that are mentioned for the microstrip lines.

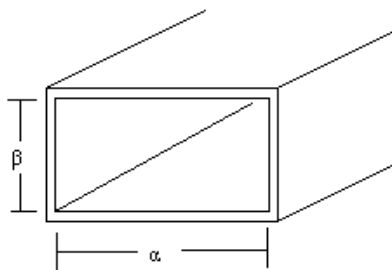


Figure 6.5: Microwave metallic orthogonal waveguide.

I joined MITAS because
I wanted **real responsibility**

The Graduate Programme
for Engineers and Geoscientists
www.discovermitas.com



Real work
International opportunities
Three work placements



Month 16
I was a construction supervisor in the North Sea advising and helping foremen solve problems





6.2.2 Transmission lines characteristics – distributed elements

A transmission line is characterized by four electrical parameters which reflect the behaviour at the steady state, provided that the construction is uniform throughout its length. These parameters are:

- Distributed inductance in series, that is expressed in H/m
- Distributed shunt capacitance in F/m
- Distributed ohmic resistance in series, that is expressed in Ω/m
- Distributed shunt conductivity, that is expressed in mho/m

The transmission lines' distributed elements can be approximately calculated for the aforementioned types of lines. Particularly, for the two parallel wires and coaxial cables, the following formulas for the distributed inductance could be used respectively:

$$L_{//} = \frac{\mu_0 \mu_r}{2\pi} \ln \frac{D^2}{r_1 r_2} \text{ in (H/m) ,}$$

where D is the distance between the parallel conductors and r_1, r_2 their radii.

$$L_{coaxial} = \frac{\mu_0 \mu_r}{2\pi} \ln \frac{D}{d} \text{ in (H/m) ,}$$

where D is the outer conductor diameter and d the core conductor thickness.

Furthermore, their distributed capacitance can be respectively calculated by the following approximate formulas:

$$C_{//} = \frac{2\pi\epsilon}{\ln\left(\frac{D^2}{r_1 r_2}\right)} \text{ in (F/m) and } C_{coaxial} = \frac{2\pi\epsilon}{\ln\left(\frac{D}{d}\right)} \text{ in (F/m) ,}$$

where ϵ is the dielectric constant of the dielectric material.

The distributed ohmic loss across the line is a significant parameter that determines the power attenuation along the line. Although it is well known that the ohmic resistance of a conductor depends on its length, its cross section and its specific resistance, at high frequencies, the skin effect should be considered as a stronger contributor to ohmic losses.

6.2.3 Telegraph equations – Characteristic impedance and transmission constant

Using the distributed parameters of a transmission line, as they are described in section 2.2, we can simulate an elementary length Δx of the line through discrete elements at a distance x from the source, as it is illustrated in Figure 6.6. In this circuit R , L , C and G are the distributed resistance, inductance, capacitance and conductivity, respectively.

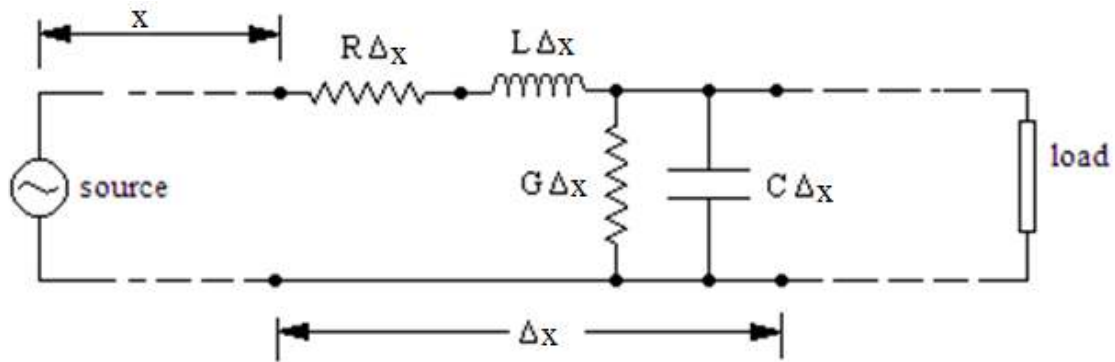


Figure 6.6: Equivalent circuit of an infinite homogeneous line's elementary length Δx .

For a sinusoidal steady state, with frequency ω , the equivalent element in series has an impedance of: $Z\Delta x = (R+j\omega L)\Delta x$, while the equivalent shunt element has an admittance of: $Y\Delta x = (G+j\omega C)\Delta x$. As a result, the equivalent circuit is that of Figure 6.7, where the current and voltage drop along the elementary length of the line could be calculated using elementary circuit laws.

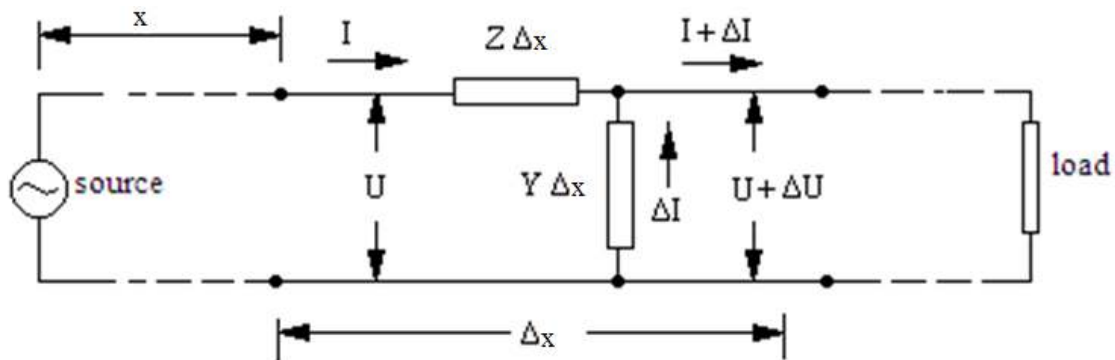


Figure 6.7: Voltage and current calculation for the equivalent circuit of Fig. 6.6.

By solving the circuit of Figure 6.7 the telegraph equations are deduced for the voltage and current along the line:

$$\frac{d^2 U}{dx^2} = ZY U \tag{6.2.1.1}$$

$$\frac{d^2 I}{dx^2} = ZY I \tag{6.2.1.2}$$

Taking into account the voltage and current initial values at the input of the line (U_0 and I_0), the solution of the equations (6.2.1.1–6.2.1.2) describe the linear combination between an incident ($e^{-\gamma x}$) and a reflected wave ($e^{\gamma x}$) as follows:

$$\begin{aligned}
 U(x) &= \frac{1}{2}(U_0 - I_0 Z_c) e^{\gamma x} + \frac{1}{2}(U_0 + I_0 Z_c) e^{-\gamma x} \\
 I(x) &= -\frac{1}{2} \left(\frac{U_0}{Z_c} - I_0 \right) e^{\gamma x} + \frac{1}{2} \left(\frac{U_0}{Z_c} + I_0 \right) e^{-\gamma x}
 \end{aligned}
 \tag{6.2.2}$$

Where, in the space of $s=j\omega$, the characteristic impedance is determined by:

$$Z_c = \sqrt{\frac{Z}{Y}} = \sqrt{\frac{R + sL}{G + sC}}
 \tag{6.2.3}$$

while the transmission constant is determined by:

$$\gamma = \sqrt{(R + sL)(G + sC)}
 \tag{6.2.4}$$

ie business school

#1 EUROPEAN BUSINESS SCHOOL
FINANCIAL TIMES 2013

#gobeyond

MASTER IN MANAGEMENT

Because achieving your dreams is your greatest challenge. IE Business School's Master in Management taught in English, Spanish or bilingually, trains young high performance professionals at the beginning of their career through an innovative and stimulating program that will help them reach their full potential.

- Choose your area of specialization.
- Customize your master through the different options offered.
- Global Immersion Weeks in locations such as London, Silicon Valley or Shanghai.

Because you change, we change with you.

www.ie.edu/master-management | mim.admissions@ie.edu | f t in YouTube



For transmission lines with a load Z_L as a termination, from equations (6.2.2) the following equations can be derived:

$$\begin{aligned} U &= U_L \left[\cosh(\gamma x') + \frac{Z_C}{Z_L} \sinh(\gamma x') \right] \\ I &= I_L \left[\cosh(\gamma x') + \frac{Z_L}{Z_C} \sinh(\gamma x') \right] \end{aligned} \quad (6.2.5)$$

In (6.2.5) the current and the voltage at the termination load have been introduced, while the distribution along the line is determined by the distance x' from the load.

Using equations (6.2.5), the input impedance at any position on the line is calculated as follows:

$$Z_{in} = Z_C \frac{Z_L + Z_C \tanh(\gamma x')}{Z_C + Z_L \tanh(\gamma x')} \quad (6.2.6)$$

6.2.4 Lossy and lossless transmission lines

From equation (6.2.4) it is deduced that the transmission constant γ is in general a complex number that can be written in the form: $\gamma = \alpha + j\beta$ where α is the attenuation coefficient and β is the phase constant. The attenuation coefficient α is expressed in Np/km, while the phase constant β , which is the imaginary part of the transmission constant, is expressed in rad/km. Particularly, the unit Np (Neper) expresses the neper logarithm of a ratio of voltages or currents. For a transmission line, the attenuation coefficient α is usually expressed in dB of power loss along the line, where the conversion of Np into dB is conducted by multiplying the factor $20 \log_{10} e = 8.686$.

For lossy transmission lines, both the transmission constant and the characteristic impedance are complex numbers, while for lossless transmission lines the transmission constant is purely imaginary ($\alpha=0$) and the characteristic impedance is purely ohmic (a real number). In order to measure both the transmission constant and the characteristic impedance of a transmission line, its input impedance for short and open termination has to be measured respectively. From (6.2.6) it is easy to derive the following calculation formula based on the aforementioned measurements:

$$Z_c = \sqrt{Z_{in}^{(oc)} Z_{in}^{(sc)}} \quad (6.2.7)$$

$$\gamma D = \frac{1}{2} \ln \frac{\sqrt{Z_{in}^{(oc)}} + \sqrt{Z_{in}^{(sc)}}}{\sqrt{Z_{in}^{(oc)}} - \sqrt{Z_{in}^{(sc)}}} \quad (6.2.8)$$

where D is the length of the transmission line and $Z_{in}^{(oc)}$, $Z_{in}^{(sc)}$ are the input impedances for open and short termination respectively. Although any type of a transmission line should have a non zero attenuation constant, for high frequencies, short lengths (usually for a fraction of the wavelength) and low loss dielectrics, are considered as lossless ($\alpha=0$). Thus, the aforementioned relations (6.2.5–6.2.6) could be simplified by substituting the hyperbolic functions with the corresponding trigonometric ones.

6.2.5 Reflection coefficient and standing waves in transmission lines

The characteristic impedance of a transmission line is of great importance, because it determines whether the reflective wave is present along the line or not. Particularly, if the termination of the line is different than the characteristic impedance, then part of the wave that is incident to the termination load is reflected back to the source. Thus, a fraction of the incident power will be transferred to the load, while the remaining power travels back to the source. The reflective wave is developed along the line and interferes with the incident wave. The result of this interference is a standing wave whose amplitude depends on the difference between the termination load and the characteristic impedance.

The standing wave is measured through the standing wave ratio (SWR) or voltage standing wave ratio (VSWR), while the reflection coefficient p determines the ratio between the reflected and incidence wave in any position of the line. The reflection coefficient at a distance x' from the load is calculated for lossy lines as follows:

$$p = \frac{Z_L - Z_C}{Z_L + Z_C} e^{-2\gamma x'} \quad (6.2.9)$$

while for lossless lines (2.9) it is modified as:

$$p = \frac{Z_L - Z_C}{Z_L + Z_C} e^{-j2\beta x'} \quad (6.2.10)$$

The standing wave ratio can be expressed through the reflection coefficient for a lossless line as follows:

$$S = \frac{1 + |p|}{1 - |p|} \quad (6.2.11)$$

In the event that the line is terminated in its characteristic impedance, the reflected wave is zero, the standing wave degenerates and the line is considered as a **matched line**. In Figure 6.8 the amplitude of the voltage standing wave is illustrated for a lossy line. In the same Figure, the voltage amplitude is also illustrated for a matched lossy line. In both cases, the apparent exponential decay is due to the attenuation through the losses along the line.

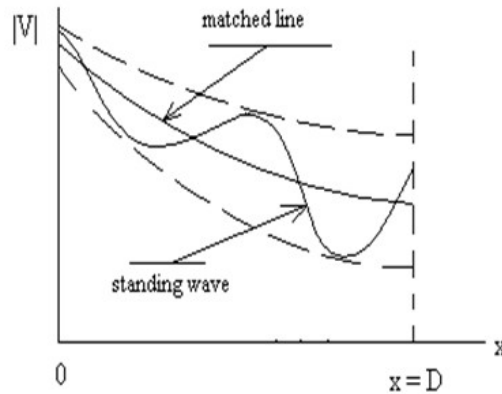


Figure 6.8: The amplitude of the voltage standing wave for a lossy line.

Furthermore, in Figure 6.9, the amplitude of the voltage standing wave is illustrated for a lossless line. This case is more important for high frequency applications when the length of the line is a few wavelengths long. Besides, the standing wave appears to be a periodic signal, with a period of half a wavelength ($\lambda/2$), whose accurate form is calculated from the assumption that at any point on the line, the voltage is $V_i + V_r = V_i(1+p)$, where V_i and V_r are the incident and reflected voltages at this point respectively.

“I studied English for 16 years but...
...I finally learned to speak it in just six lessons”
Jane, Chinese architect

ENGLISH OUT THERE

Click to hear me talking before and after my unique course download

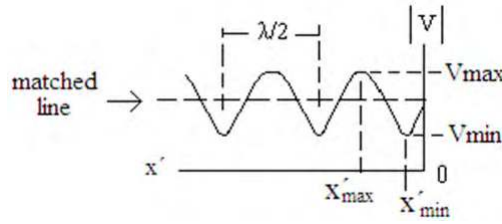


Figure 6.9: The amplitude of the voltage standing wave for a lossless line.

Particularly, the voltage amplitude along the line is calculated as follows:

$$|V| = |V_i| \sqrt{1 + 2|p| \cos \varphi + |p|^2} \tag{6.2.12}$$

where, $\varphi = \theta - 2\beta x'$, $\theta = \angle p_L = \angle \frac{Z_L - Z_C}{Z_L + Z_C}$ and $\beta = \frac{2\pi}{\lambda}$. The expression (2.12) is periodic in x' with a period of $\lambda/2$, while its maximum and minimum values are:

$$|V_{\max}| = |V_i|(1 + |p|) \quad |V_{\min}| = |V_i|(1 - |p|) \tag{6.2.14}$$

Moreover, the first local maximum will be found at a distance: $x'_{\max} = \lambda \left[\frac{\theta}{4\pi} - \frac{k}{2} \right]$ from the termination load (with $k = 0, \pm 1, \pm 2, \dots$) and the successive local minimum x'_{\min} is located at a distance of $\lambda/4$ from the respective local maximum.

6.2.6 Power transfer from source to load

The standing wave along a transmission line is actually created from the interference between the incident and the reflected waves of voltage or current. Due to this phenomenon, the standing wave traps a fraction of the power that is transferred through the incident wave towards the load. As a result, the power that the termination load could dissipate is limited from the existence of the standing wave along the line. For a lossless line, the power that is dissipated from the load is calculated as follows:

$$P = \frac{|V_i|^2}{2Z_C} (1 - |p|^2) = P_i (1 - |p|^2) \tag{6.2.15}$$

The expression (6.2.15) determines that the fraction of the power that is trapped in the standing wave is $|p|^2$ and becomes zero when the reflection coefficient becomes zero. This is actually the reason why a transmission line has to be matched. Apparently, a matched line carries no reflective waves and consequently the reflection coefficient is zero. As a result, the incident power at its input will arrive and be dissipated in the load without any loss inside the transmission line due to reflections. Herein, it has to be clarified that the loss of power due to standing wave trapping, is different than the one that is derived from the ohmic losses along the line.

The aforementioned analysis has considered that the internal impedance of the source or the generator is equal to the line's characteristic impedance. This assumption enables the development of a standing wave only from the reflection at the line's termination load. However, in many applications, both the source's internal impedance and the termination load could be different than the line's characteristic impedance. In this case, the standing wave is developed from successive reflections from both the input side and the termination load.

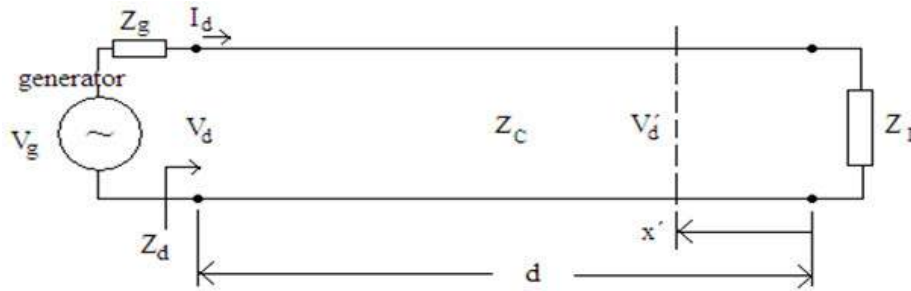


Figure 6.10: A doubly terminated transmission line.

For a doubly terminated transmission line (Figure 6.10), the power transfer from the generator to the load is now calculated as follows:

$$P = \left| \frac{V_g}{(Z_g + Z_C)(1 - p_d p_g)} \right|^2 \frac{Z_C}{2} (1 - |p_L|^2) \tag{6.2.16}$$

where,

$$p_d = \frac{Z_d - Z_C}{Z_d + Z_C}, \quad p_g = \frac{Z_g - Z_C}{Z_g + Z_C} \tag{6.2.17}$$

Evidently, with $Z_g = Z_C$, the expression (6.2.16) results to expression (6.2.15).

6.2.7 Quarter and half wavelength transmission lines

Energy trapping along a transmission line due to standing waves is not always a phenomenon that has to be avoided. Indeed, high frequency applications can take advantage of the energy trapping phenomena in short or open circuited lines in order to develop either inductive or capacitive elements or even more commonly, to use them as high frequency resonators.

The critical parameters for the development of high frequency elements using a particular type of a transmission line are the length (in wavelengths) and the termination load. More particularly, for a line with a length d , less than a quarter wavelength, zero or negligible losses and short circuited end (a shorted line also called a stub), the input impedance is calculated as follows:

$$Z_{in} = Z_C j \tan(\beta d) \tag{6.2.18}$$

Since the tangential argument is less than $\pi/2$ ($2\pi d/\lambda < \pi/2$) and Z_c is a real number, the expression (6.2.18) represents an equivalent impedance of a perfect inductor (Figure 6.11).

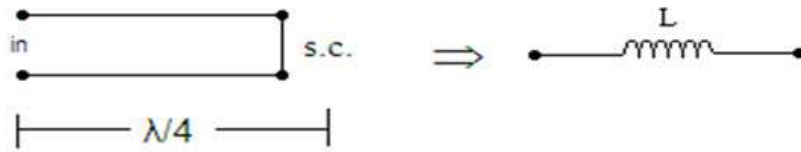


Figure 6.11: A short circuited transmission line with length less than a quarter wavelength, is equivalent with a perfect inductor.

For a corresponding line with a length d , less than a quarter wavelength, zero or negligible losses and open end, the input impedance is calculated as follows:

$$Z_{in} = \frac{Z_c}{j \tan(\beta x')} = -j \frac{Z_c}{\tan(\beta x')} \tag{6.2.19}$$

Since the tangential argument is less than $\pi/2$ ($2\pi d/\lambda < \pi/2$) and Z_c is a real number, the expression (6.2.19) represents an equivalent impedance of a perfect capacitor (Figure 6.12).

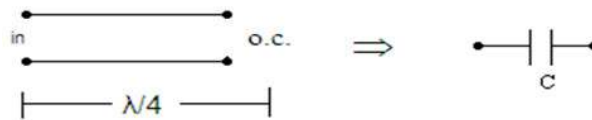


Figure 6.12: An open circuited transmission line with length less than a quarter wavelength, is equivalent with a perfect capacitor.

Excellent Economics and Business programmes at:



**university of
 groningen**



**“The perfect start
 of a successful,
 international career.”**

CLICK HERE
 to discover why both socially
 and academically the University
 of Groningen is one of the best
 places for a student to be

www.rug.nl/feb/education



The properties now of a line with length equal to a quarter wavelength are based on its input impedance that is calculated as follows:

$$Z_{in}^{(\lambda/4)} = \frac{Z_C^2}{Z_L} \tag{6.2.20}$$

If the quarter wavelength line is shorted at its end ($Z_L=0$) then the input impedance is infinite, $Z_{in} = \infty$. Consequently, a quarter wavelength transmission line with a shorted end is equivalent with an L//C resonator (see Figure 6.13). Furthermore, for a quarter wavelength transmission line with an open end ($Z_L=\infty$), the input impedance is zeroed, $Z_{in}=0$, and its equivalent circuit is an L,C resonator in series.

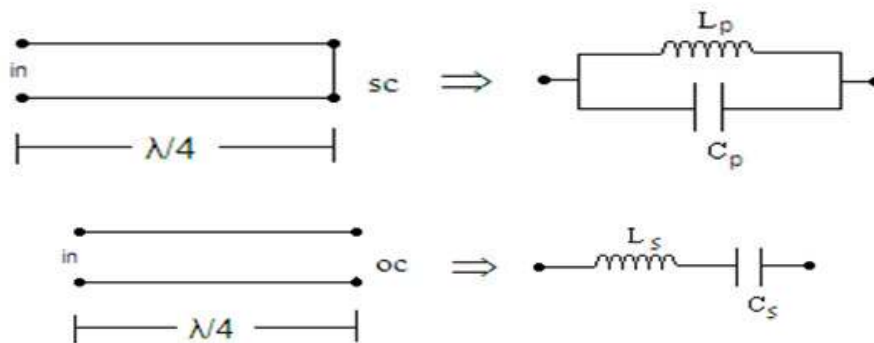


Figure 6.13: An open and short circuited transmission line with length equal to a quarter wavelength, as a resonator.

The resonance properties of the quarter wavelength lines have a wide application in resonance passive structures of RF and microwave networks. However, the standing wave form of Figure 6.13, provides resonance condition not only for the fundamental frequency but also for all its odd multiples. The odd multiples of the fundamental frequency are the well known **overtone** frequencies and they are present in any application of a quarter wavelength transmission line, which operates as a resonator in high frequencies.

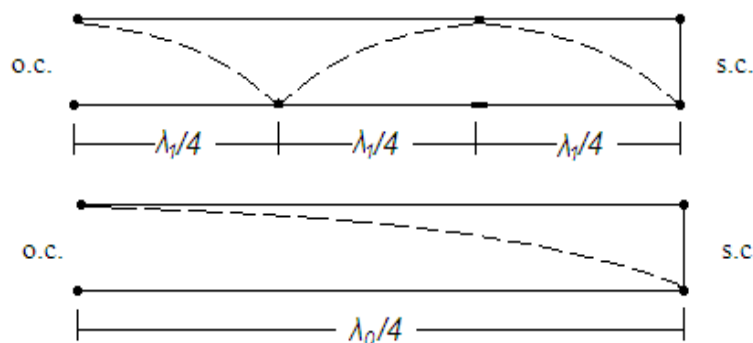


Figure 6.14: The standing wave along a shorted line in its fundamental and 3rd overtone resonance.

The resonance only for the odd overtones could be easily explained through the boundary conditions for the voltage at the two line terminations. Particularly, the line's open and short terminations, require maximum and zero voltage at the ends respectively.

In addition to the aforementioned analysis for a quarter wavelength line, similar results can be derived for a half wavelength transmission line. For a half wavelength line, the input impedance is equal with its load consequently, its self resonance appears when the line is terminated at open or short circuit at both ends. The overtones for a half wavelength line are all multiples of the fundamental frequency.

6.2.8 Smith Chart application on transmission lines

The Smith chart is a graphical method designed to calculate the functional characteristics of a transmission line. The need for the use of this method resulted from the complexity of the analytical calculations. The method is particularly useful in laboratory applications, where there is a need for fast and accurate calculations. The chart was published by the engineer P.H. Smith in 1939 and is designed on the domain of the reflection coefficient p . Through the chart, we can extract information about the line's input impedance, the coefficients of reflection and the standing wave. On the Smith chart, the reflectance at any point of the line is considered as a complex number in its cartecian form:

$$p = u + jv \quad (6.2.21)$$

Every point on the chart represents a normalized impedance, i.e. the input impedance of the line, at each point of it, normalized in respect to the line's characteristic impedance:

$$Z_n = \frac{Z}{Z_C} = \frac{R}{Z_C} + j \frac{X}{Z_C} = r + jx \quad (6.2.22)$$

There is analytical proof that the parameters u, v, r and x , are related to each other with the following equations that represent circles:

$$\left(u - \frac{r}{r+1}\right)^2 + v^2 = \frac{1}{(r+1)^2} \quad (6.2.23)$$

$$(u-1)^2 + \left(v - \frac{1}{x}\right)^2 = \frac{1}{x^2} \quad (6.2.24)$$

The equation (2.23) determines circles with centers at the points $u = \frac{r}{r+1}$, $v=0$ and radii $\frac{1}{r+1}$ (Figure 6.15). Every point on each circle is characterized by a constant r (r is ohmic part of the normalized impedance). All circles are tangent at point $u=1$, $v=0$, which represents $r=\infty$, while the outer circle represents all points with $r=0$. The circle $r=1$ is the matching circle, because it passes from the coordinates center, which is the point that represents the characteristic impedance. It is remarkable that all potential impedances can be represented by a point inside the outer circle $r=0$, consequently the Smith chart is enclosed by the outer circle.

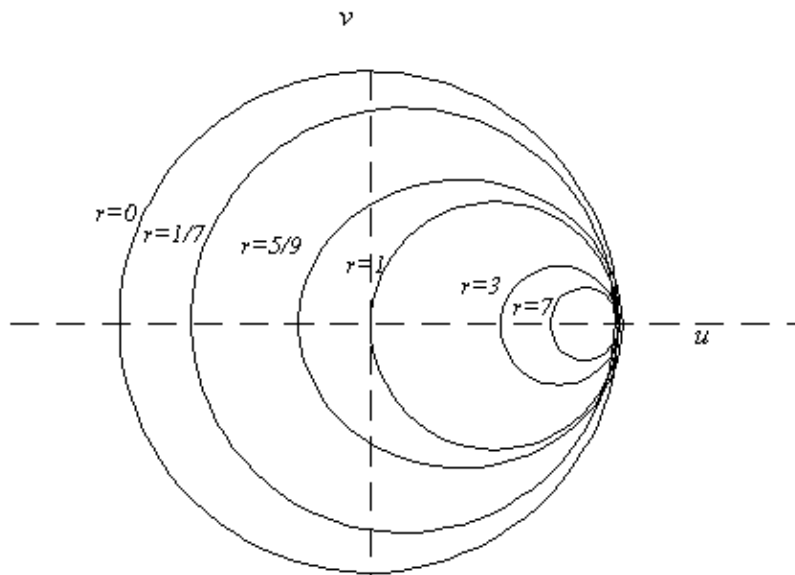


Figure 6.15: Circles that represent points on the chart with equal r .

The equation (6.2.24) determines circles with centers at the points $u=1$, $v = \frac{1}{X}$ and radii $\frac{1}{X}$. The centers of these circles lie on the line $u = 1$, and their arcs that are cut off from the outer circle of the chart, represent points with a constant imaginary part of impedance of the line.

LIGS University

based in Hawaii, USA

is currently enrolling in the
Interactive Online **BBA, MBA, MSc,**
DBA and PhD programs:

- ▶ enroll **by October 31st, 2014** and
- ▶ **save up to 11%** on the tuition!
- ▶ pay in 10 installments / 2 years
- ▶ Interactive **Online** education
- ▶ visit www.ligsuniversity.com to find out more!

Note: LIGS University is not accredited by any nationally recognized accrediting agency listed by the US Secretary of Education. More info [here](#).





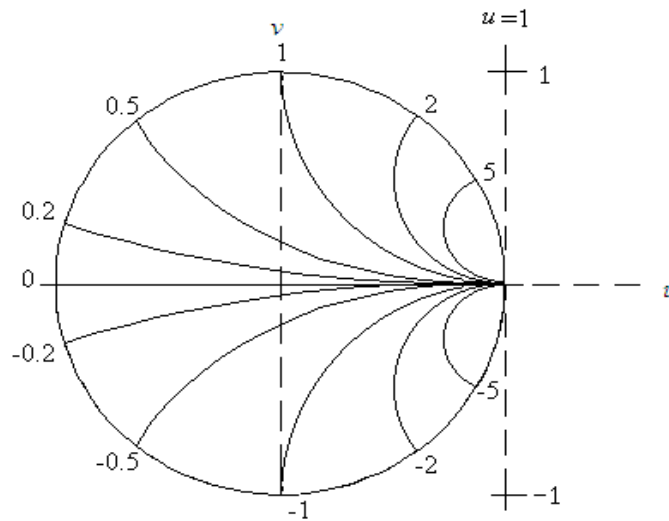


Figure 6.16: Circular arcs that represent points on the chart with equal x .

For $x=0$ (pure ohmic resistance) the corresponding arc degenerates into a straight line, while for $x=\infty$ (an infinite reactive part of the line's impedance) the corresponding arc degenerates into the point $u=1, v=1$. It is clarified here that the positive values of x (inductive loads) are placed in the upper semicircle, while the negative (capacitive loads) in the lower semi-circle.

The final version of the chart is that of Figure 6.17, where the bundles of circular arcs and circles are plotted in a dense grid. Therein, each constant r circle and each arc with constant x can be easily determined. Outside the chart's boundary circle, there is a concentric circle with external and internal ratings. The outer scales determine distances that correspond to movement toward generator (clockwise) and are expressed in wavelengths, while the internal ratings correspond to movement toward load (anticlockwise).

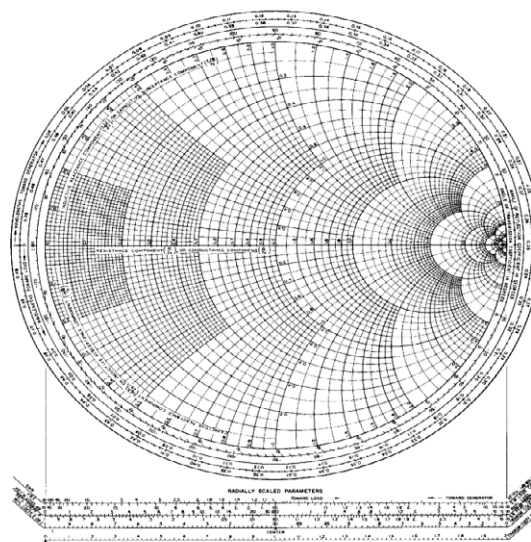


Figure 6.17: The complete form of the Smith chart.

For a lossless transmission line with given characteristic impedance Z_C and termination load Z_L , the normalized termination load will be equal to $Z_L/Z_C = r+jx$ (point A in Figure 6.18); this is the “location of the load on the chart”. The circle (0,0A) represents the lossless transmission line (line’s circle). Moving along this circle, the line’s input impedance can be determined from the location of each point on the circle (corresponding r and x values).

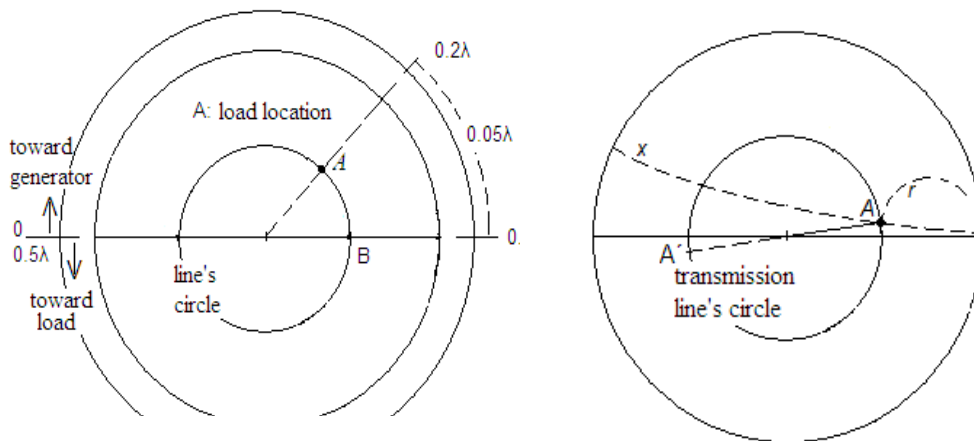


Figure 6.18: (Left) The circle of a lossless line – (Right) Covering distances along the line.

The Smith chart is useful for the study of the input impedance along the line. By covering a distance equal to e.g. 0.05λ from the load (see Fig. 6.18 –right side), we meet point B of the line. This point determines the input impedance of the line by reading its corresponding r and x values. Moreover, point B provides the value of VSWR that is readable on the horizontal axis. Consequently, as the line’s circle gets smaller, the standing wave also decreases. Ideally, the perfect match can be achieved if the line’s circle creates a single point at the center of the chart.

6.3 Coaxial cable T-resonator measurements results

A coaxial cable T-resonator (M. Dirix, 2012) (Y.H. Chou, 2008), is a two-port setup that uses two 50Ω coaxial cables, with a parallel connected coaxial resonating transmission line. This line should be either an open-ended quarter wavelength or a short-ended, half wavelength stub. Using a 50Ω Network Analyzer (Figure 6.19) and connecting its input and output ports to the ports of the T-resonator setup, we can analyze its frequency response for the UHF frequency range. A Network Analyzer (VNA) is a very common instrument for frequency analysis response of a passive network in RF. Particularly, the instrument’s output operates as a frequency generator that scans a frequency-range defined by the user. The produced frequencies are driven through the passive network under test whose output is detected by the Network Analyzer’s input. Internally, the instrument compares the input and output signals and displays the response of the passive network.

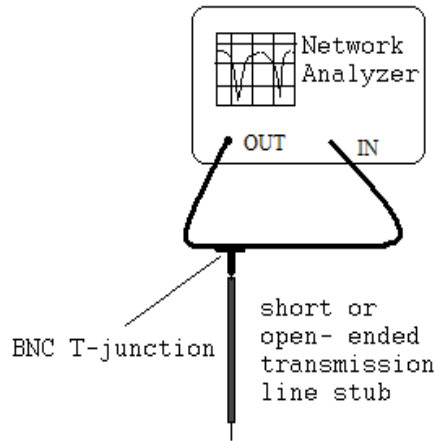



Figure 6.19 : Measurement setup using a 50Ω Network Analyzer.

If we use a resonating short-ended coaxial cable stub for the half wavelength frequency, as well as for its integer multiples, the stub’s input appears to be a short circuit (for a half wavelength line with short-circuit termination, the input impedance is zero). The same effect also appears when we use an open-ended coaxial cable for the quarter wavelength frequency and its odd integer multiples (for a quarter wavelength line with open termination, the input impedance is zero). As a result, for these discrete frequencies, a strong attenuation will appear on the Network Analyzer’s input port.

.....Alcatel-Lucent 

www.alcatel-lucent.com/careers

What if you could build your future and create the future?

One generation’s transformation is the next’s status quo. In the near future, people may soon think it’s strange that devices ever had to be “plugged in.” To obtain that status, there needs to be “The Shift”.



If we assume a lossless coaxial cable, then we can analyze theoretically the proposed T-resonator two-port frequency response, by using the lossless transmission line theory. The frequency analysis for a short-ended stub with 0.5m length and 66.6% propagation velocity, is illustrated in Figure 6.20. Each resonance frequency is an integer multiple of the fundamental f_0 which can be calculated as follows:

$$f_0 = \frac{c_0}{2\ell\sqrt{\epsilon_r}} \tag{6.3.1}$$

where for propagation velocity 66.6% , $\sqrt{\epsilon_r} = 1.5$ and ℓ is the stub's physical length.

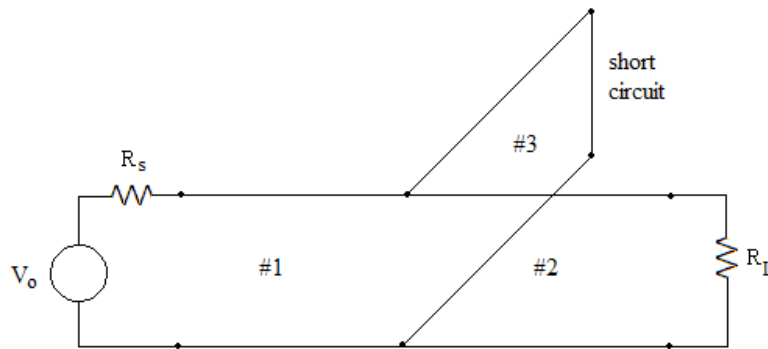


Figure 6.20: The equivalent lossless transmission line circuit.

By considering the instrument internal impedance $R_s=50\Omega$, the power loss from input to output can be calculated as follows:

$$Loss(dB) = 10 \log(1 - |p|^2), \tag{6.3.2}$$

where the reflection coefficient is provided by the standing wave along line #1, while line #2 is matched. Consequently, the calculation of p for short-ended line #3, is as follows:

$$p = \frac{Z_L - Z_c}{Z_L + Z_c}, \text{ with } Z_L = Z_c // jZ_c \tan(\beta d) = \frac{jZ_c \tan(\beta d)}{1 + j \tan(\beta d)}. \tag{6.3.3}$$

whereas, for open-ended line #3 the reflection coefficient p is calculated as follows:

$$p = \frac{Z_L - Z_c}{Z_L + Z_c}, \text{ with } Z_L = Z_c // Z_c / j \tan(\beta d) = \frac{Z_c}{1 + j \tan(\beta d)}. \tag{6.3.4}$$

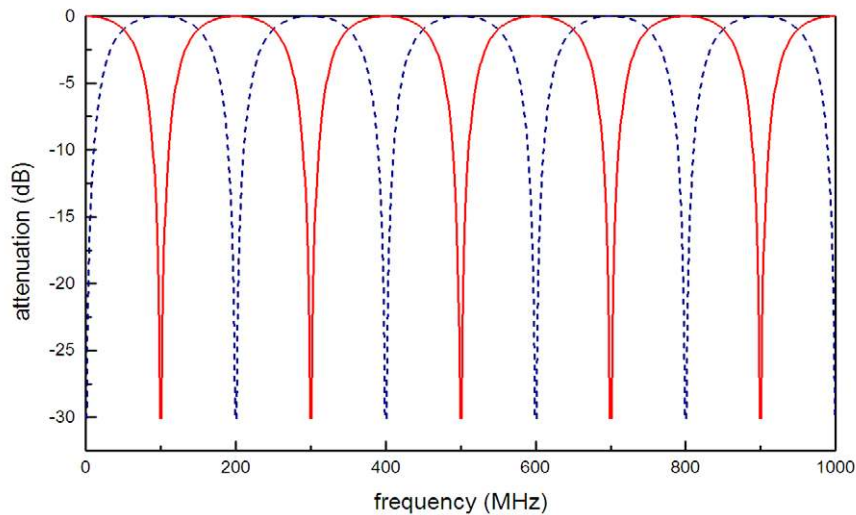


Figure 6.21: T-resonator frequency response for lossless transmission lines with 66.6% propagation velocity and a 0.5m parallel connected coaxial cable with short termination (dashed line), and open termination (solid line).

In the context of the above described theoretical framework and due to the absence of attenuation losses along the lines, the Q factor for each resonance appears to be infinite. Evidently, this result can be obtained from the determination of the loaded Q factor ($Q_L = f / BW_{3dB}$), where for a lossless resonance, BW_{3dB} tends to a zero limit value (see also Figure 21). Apparently, finite Q factors for lossy transmission lines are expected.

6.3.1 Coaxial Cable Experimental Measurements and Results

Next, using the aforementioned setup, we measure the frequency response of two coaxial cable stubs (half wavelength) with 0.5m length, the one with a copper shield and the other with an electrotexile shield (Vassiliadis, 2011). In Figure 6.22 (a) and (b), the Network Analyzer's frequency response snap shots are illustrated for both the copper shield and the electrotexile shield coaxial cables, respectively. The finite depth of the resonance nulls indicates the level of attenuation losses, whereas the 3 dB bandwidth, the Q factor value. The basic remark from Figure 6.23 (a) is that the loaded Q for the first 4 resonance frequencies is approximately the same, whereas, in Figure 6.23 (b), the second resonance frequency has an evidently higher Q. In particular, from Figure 6.23 (b), we notice that the electrotexile coaxial cable presents a Q comparable with that of the corresponding copper coaxial cable, but only for the resonance frequency of 400MHz.

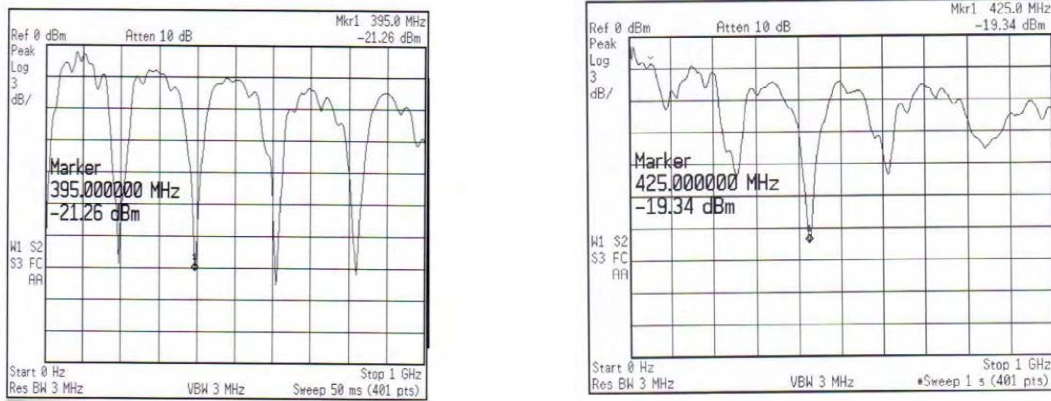


Figure 6.22: (a) Frequency response of a coaxial 'T' resonator with a copper shield and (b) Frequency response of a coaxial 'T' resonator with an electrotextile shield.

In Figure 6.22 (a) and (b) the resonance response around 400MHz is illustrated for a smaller frequency span, in order to measure the 3dB bandwidth and the maximum attenuation level more accurately.



Maastricht University

Leading in Learning!

Join the best at the Maastricht University School of Business and Economics!

Top master's programmes

- 33rd place Financial Times worldwide ranking: MSc International Business
- 1st place: MSc International Business
- 1st place: MSc Financial Economics
- 2nd place: MSc Management of Learning
- 2nd place: MSc Economics
- 2nd place: MSc Econometrics and Operations Research
- 2nd place: MSc Global Supply Chain Management and Change

Sources: Keuzegids Master ranking 2013; Elsevier 'Beste Studies' ranking 2012; Financial Times Global Masters in Management ranking 2012

Maastricht University is the best specialist university in the Netherlands (Elsevier)

Visit us and find out why we are the best!

Master's Open Day: 22 February 2014

www.mastersopenday.nl



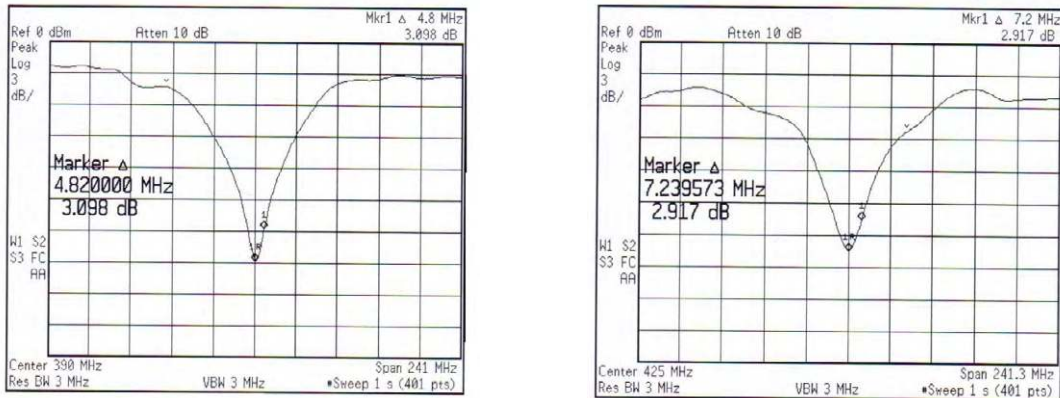


Figure 6.23: (a) Notch characteristics for a coaxial 'T' resonator with a copper shield
 (b) Notch characteristics for a coaxial 'T' resonator with an electrotextile shield.

Using the same span settings we measure the relative 3dB bandwidth and the maximum attenuation for the first three resonance frequencies of the T-coaxial resonators. In Table1 the measurement results are tabulated, considering that the reference instrument power is 0dBm.

	Coaxial cable with copper shield				Coaxial cable with textile shield		
	f (MHz)	L_A (dB)	BW(MHz)	Q_L	f' (MHz)	L_A' (dB)	BW'(MHz)
F_0	200	-20	+/-2.5	40	250	-12	+/-25
$2F_0$	400	-21	+/-4.8	41.6	425	-19	+/-7.2
$3F_0$	600	-22	+/-5	60	620	-12	+/-12

Table 1: Tabulated measurement results for the copper reference cable and the cable with conductive textile shield under test.

Evidently, from Table 1, in the first three resonance frequencies of the copper coaxial cable, the loaded Q slightly increases at higher frequencies, whereas for the electrotextile, the higher Q appears only at the second overtone (400MHz).

Consequently, it is reasonable to examine the attenuation characteristics of the electrotextile coaxial cable in this range of frequencies.

6.3.2 Calculation of the electrotextile coaxial cable attenuation constant

From the measurement results of Table 1 we can calculate the unloaded Q factor for the 400MHz resonance frequency as follows (M. Dirix, 2012):

$$\text{for the copper coaxial cable: } Q_0 = \frac{Q_L}{\sqrt{1 - 2 \times 10^{L_A/10}}} = 41.3 \tag{6.3.5.1}$$

$$\text{for the electrotextile coaxial cable: } Q'_0 = \frac{Q'_L}{\sqrt{1 - 2 \times 10^{L'_A/10}}} = 29.9 \tag{6.3.5.2}$$

The unloaded quality factors from expressions (6.3.5) comprise of the loss effect from the conductors and the dielectric losses, since radiation losses are negligible:

$$\frac{1}{Q_0} = \frac{1}{Q_c} + \frac{1}{Q_d} \quad (6.3.6.1)$$

$$\frac{1}{Q'_0} = \frac{1}{Q'_c} + \frac{1}{Q_d} \quad (6.3.6.2)$$

where, Q_c is the quality factor of the conventional cable due to copper conductor losses, Q'_c is the quality factor that corresponds to the losses of the cable shielded by an electrotexile, and Q_d is the quality factor due to dielectric losses, which are common for both cables. From expressions (3.6) the quality factor due to electrotexile losses, is calculated through the unloaded Q of both resonators as follows:

$$\frac{1}{Q'_c} = \frac{1}{Q_c} - \left[\frac{1}{Q_0} - \frac{1}{Q'_0} \right] \quad (6.3.7)$$

For a smooth copper coaxial cable RG58 C/U, we calculate the quality factor which corresponds to copper conductor losses, as follows:

$$Q_c = \frac{\beta}{2a_c} = \frac{\pi\sqrt{\epsilon_r}}{\lambda_0 a_c}, \quad (6.3.8)$$

where a_c is the copper conductor attenuation constant which is calculated as follows for a coaxial cable (Pozar, 2005) :

$$a_c = \frac{R_s}{2\eta \ln\left(\frac{b}{a}\right)} \left(\frac{1}{a} + \frac{1}{b} \right) \quad (6.3.9)$$

In (6.3.9), parameters a and b are the core and shield radii. For the RG58 C/U cable $a=1\text{mm}$ and $b=4\text{mm}$, whereas $\sqrt{\epsilon_r} = 1.5$ and $\eta = \frac{120\pi}{\sqrt{\epsilon_r}} \Omega$ is the impedance of the dielectric insulator. The surface resistivity R_s of the copper conductor could be calculated by considering the skin effect depth $\delta_s = \sqrt{2/\omega\mu\sigma}$ from the expression:

$$R_s = \frac{1}{\sigma\delta_s} = \sqrt{\frac{\omega\mu_0}{2\sigma}} \quad (6.3.10)$$

Considering smooth copper conductor with $\sigma = 5.813 \times 10^7 \text{ S/m}$ we calculate the attenuation constant as $a_c = 3.6 \times 10^{-3} \text{ Np/m} = 0.03 \text{ dB/m}$. The relative Q_c that is then calculated from (6.3.8) is ≈ 1745 and is valid only for smooth copper conductors. Taking into account the conductor's surface roughness and the woven type of the shield conductor, the aforementioned value of quality factor is significantly reduced. However, its final value should be higher than the quality factor of resonators unloaded Q ($Q_c \gg Q_0, Q'_0$) and the following approximation is justified:

$$\frac{1}{Q'_c} \cong \frac{1}{Q_0} - \frac{1}{Q'_0} \Rightarrow Q' = 108 \quad (6.3.11)$$

As a result, from (6.3.11) and (6.3.8) we calculate the attenuation constant for the electrotexile coaxial cable: $a'_c = 0.058 \text{ Np/m} = 0.5 \text{ dB/m}$.

Download free eBooks at bookboon.com

6.4 Microstrip T-resonator measurements results

An alternative measurement setup layout for the evaluation of electrotile materials in RF frequencies is proposed herein. The coaxial lines that have been examined in section 3 of this chapter, are replaced by microstrip lines. The proposed layout is illustrated in Figure 6.24 and consists of a copper microstrip line that connects the input and output of the Network Analyzer through SMA connectors. In the middle of the copper microstrip line, an open-ended line is connected, with its upper conductor consisting of a conductive textile material.

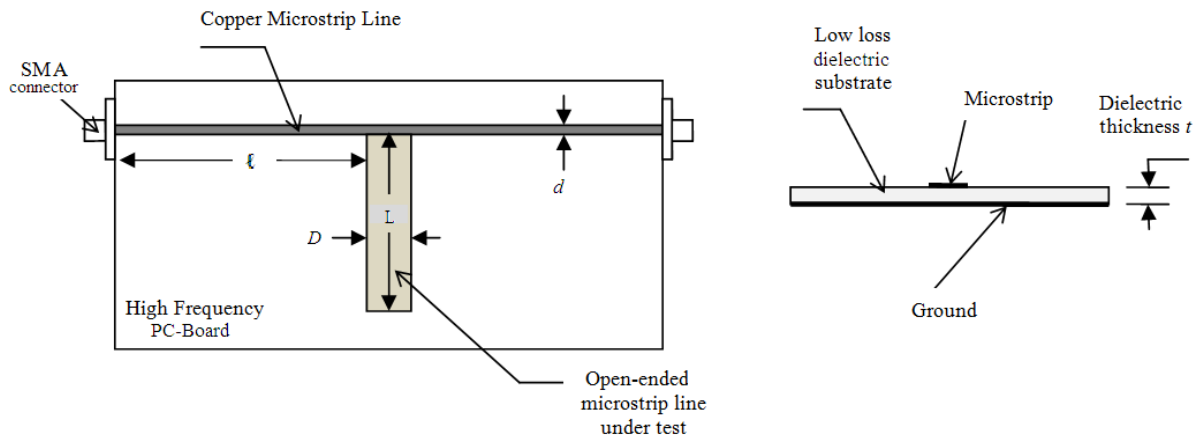


Figure 6.24: A microstrip T-resonator layout (left) and its cross section (right).

> Apply now

REDEFINE YOUR FUTURE
AXA GLOBAL GRADUATE PROGRAM 2015

redefining / standards

agence.cdg © Photonistop



According to the analysis that is presented in the previous section, a similar frequency response using the same calculation scheme is expected. Moreover, the proposed layout should be more adequate for a measurement setup, despite the expected difficulties of copper-textile connection and the adhesion between the textile and the dielectric substrate.

6.4.1 Design and analysis

The characteristic impedance of a microstrip line depends on the thickness and the dielectric constant of the low-loss dielectric substrate; the width of the upper conductor; as well as the thickness of the conductive material. The pc-board material is selected with $\epsilon_r=10$ and thickness $t=1.2\text{mm}$, while the copper microstrip line is 5mm wide ($d=5\text{mm}$) and 30cm long ($\ell=15\text{cm}$). The calculation of the characteristic impedance for the aforementioned data, gives an approximate value of $Z_c=20\Omega$. Although for matching with the Analyzer's ports' impedance the characteristic impedance should be 50Ω , this is not always achieved. In order to increase the characteristic impedance Z_c the thickness t should be increased or the width d should be decrease. However, due to practical limitations, Z_c could be different than the matching impedance.

Regarding the open-ended line under test, its width $D=1\text{cm}$ and its length $L=15\text{cm}$. These dimensions have been considered as suitable for the evaluation of conductive textile pieces in RF frequencies. However, precautions should be taken, in order to keep the conductive item stick on the pc-board. For this reason, a double sided tape could be used, or another adhesive method that keeps the item in contact with the substrate. Using the aforementioned dimensions and considering initially a copper conductor, the characteristic impedance should be approximately 12.5Ω .

As far as the analysis is concerned, we adopt the circuit that describes the problem, if $R_s=R_1=50\Omega$, the characteristic impedance of lines #1 and #2 is 20Ω and the characteristic impedance of line #3 is 12.5Ω with its termination open. In the event that the calculation takes into account the connection cables without any calibration procedure that compensates their involvement, then the formulation of expressions (6.2.16–6.2.17) is required.

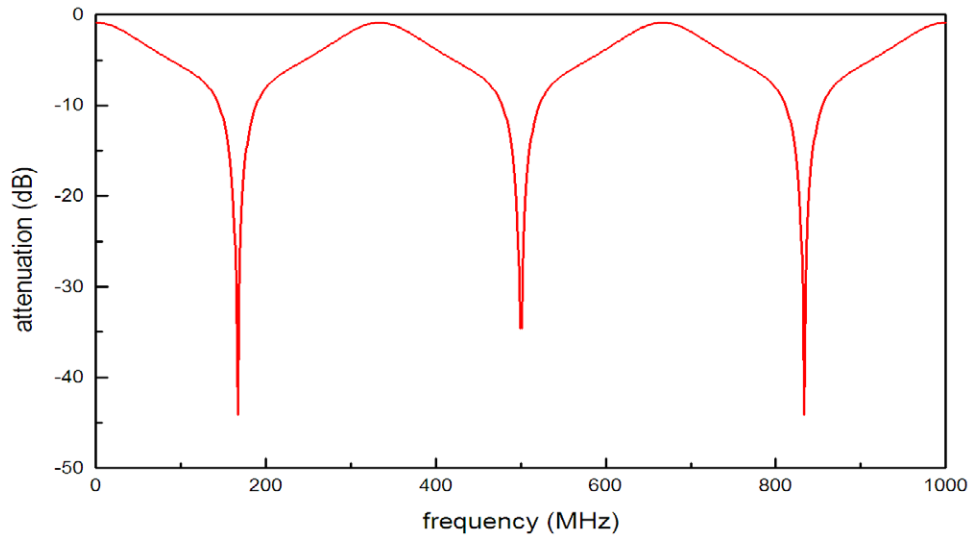


Figure 6.25: T-resonator frequency response (see details in the text).

However, the VNAs can be calibrated either manually or automatically. The calculations could be simplified and based on the procedure that is described through expressions (6.3.2–6.3.5). As a result of the application of the latter procedure, the frequency response is illustrated in Figure 6.25.

It is evident from the analysis, that the frequencies of resonance are independent from the characteristic impedance of lines #1 and #2. The fundamental frequency of resonance, is at approximately 170MHz for copper conductors and lossless dielectric materials, and also supports all odd overtone frequencies.

6.4.2 Experimental Measurements and Results

The aforementioned layout has been prepared and tested with a high frequency Network Analyzer within the 0 to 1.5GHz frequency range. The test is conducted for a copper open-ended line in order to register the measurements as reference. It is necessary to calibrate the instrument for the measurement, in order to isolate any discrepancies from the connections through the test cables. The calibration procedure could be conducted either manually or automatically (electronic calibration) for the new generation of VNAs.

The frequency response is illustrated in Figure 6.26 and it is evident that there is a good agreement with the theoretical results. However, a drift of frequency toward higher frequencies is observed (the theoretical fundamental frequency is 170MHz, whereas the measured is 205MHz). This drift is justified by the imperfect way the copper open-ended line has been positioned on the dielectric substrate (a copper strip on a double sided tape has been used). Specifically, areas where the copper leaves a void between its surface and the substrate, reduce the effective dielectric constant ϵ_r . Therefore, the fundamental and the overtone frequencies will drift upwards, as it is predicted by expression (6.3.1). As it will appear later on, this discrepancy will be more intensive for the textile conductor, because its texture enhances the aforementioned effect. Although, this is an inconvenient remark for the measurement setup, it will not affect the measurement of the quality factor (as described in section 6.3).

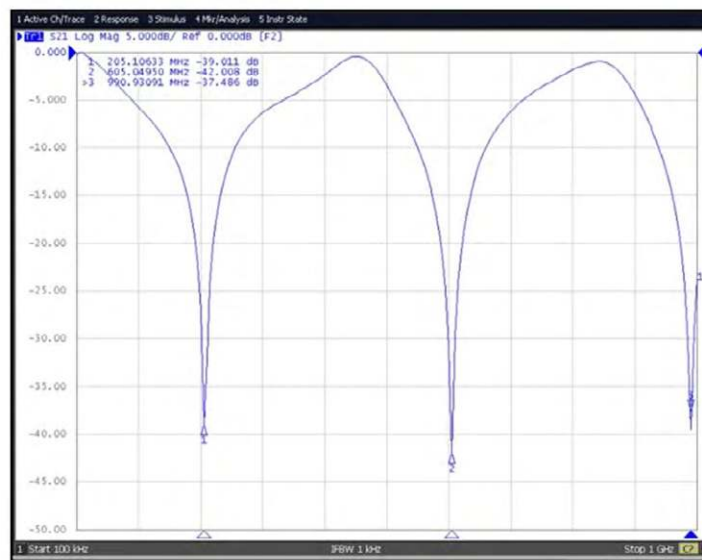


Figure 6.26: Frequency response for copper open-ended line under test.

In Figure 6.26 supplementary information about the transmission line circuitry has been provided. Specifically, the Smith chart for the input impedance is illustrated. There is no line crossing the center of the chart and the input is not matched at 50Ω, as confirmed theoretically. However, for the resonance frequency (see marker 1) the input impedance is close to the infinity point of the chart.

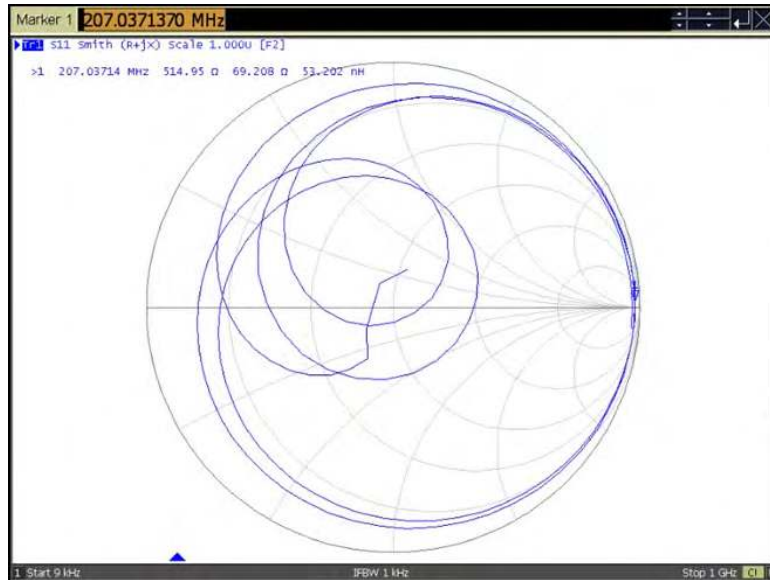


Figure 6.27: The Smith chart for the input impedance with copper open-ended line under test.

In Figure 6.27, the Smith chart for the input-output impedance is illustrated. Since the output impedance that is seen from the instrument’s port at the resonance frequencies is approximately 50Ω , the corresponding instrument port is matched (notice that $2\ell=\lambda/2$). Consequently, three lines are crossing the center of the chart and correspond to the three resonance frequencies that are captured by the instrument’s frequency span.

BI NORWEGIAN BUSINESS SCHOOL

EFMD **EQUIS ACCREDITED**

Empowering People. Improving Business.

BI Norwegian Business School is one of Europe’s largest business schools welcoming more than 20,000 students. Our programmes provide a stimulating and multi-cultural learning environment with an international outlook ultimately providing students with professional skills to meet the increasing needs of businesses.

BI offers four different two-year, full-time Master of Science (MSc) programmes that are taught entirely in English and have been designed to provide professional skills to meet the increasing need of businesses. The MSc programmes provide a stimulating and multi-cultural learning environment to give you the best platform to launch into your career.

- MSc in Business
- MSc in Financial Economics
- MSc in Strategic Marketing Management
- MSc in Leadership and Organisational Psychology

www.bi.edu/master



Next, the copper conductor is replaced by a conductive textile material with the same dimensions. The frequency response is illustrated in Figure 29. Therein, six different lengths (15, 14, 13, 12, 11 and 10cm) have been tested and their fundamental frequency corresponds to markers 1 to 6 respectively.

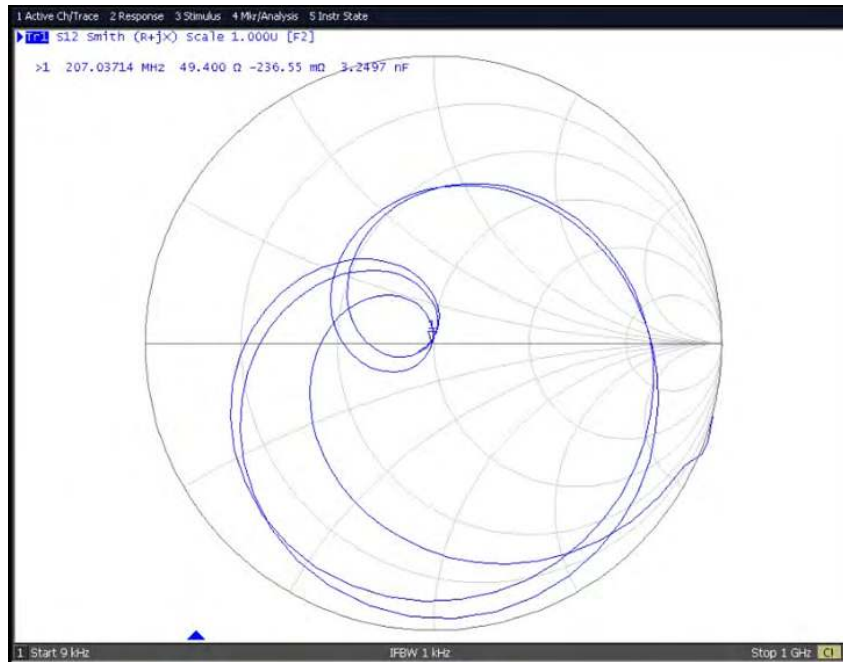


Figure 6.28: The Smith chart for the input-output impedance with copper open-ended line under test.

Evidently, and due to the aforementioned effect, the frequencies are found higher than the copper and quite higher than the theoretical. However, the Q factor can be easily measured through the bandwidth and the center resonance frequency.

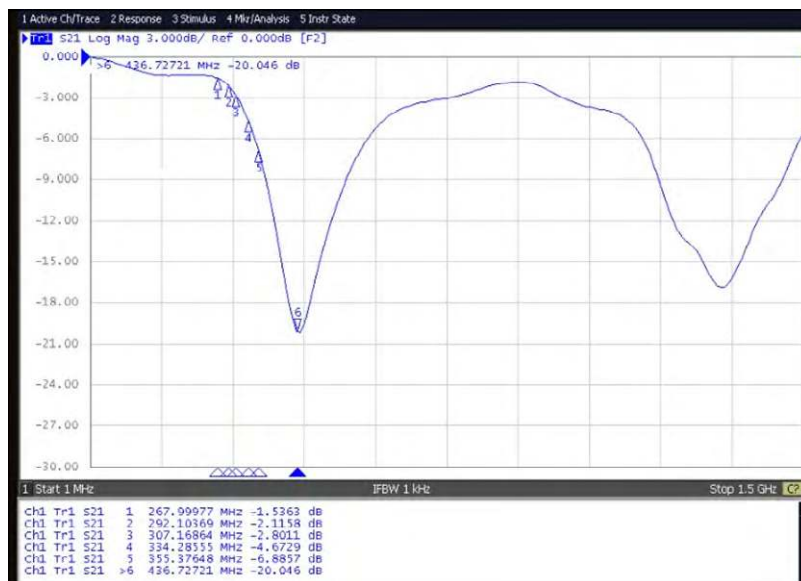


Figure 6.29: Frequency response for textile open-ended line under test and 4 different lengths.

6.5 Antenna fundamentals

6.5.1 Radiation mechanism

In essence, antennas are devices that transform an electric current or voltage on a conductive material to an electromagnetic wave propagating in the air, or vice versa. The IEEE definition of antennas includes the transmission or reception of electromagnetic waves (S.P. Savvaidis, 2011). Nevertheless, antennas may also transmit and receive electromagnetic waves in the vacuum or other dielectric environments, as illustrated in Figure 6.30.

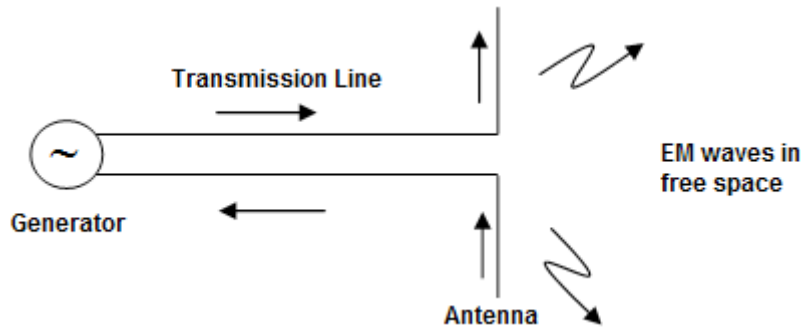


Figure 6.30: A simplified diagram of an antenna connected to a transceiver.

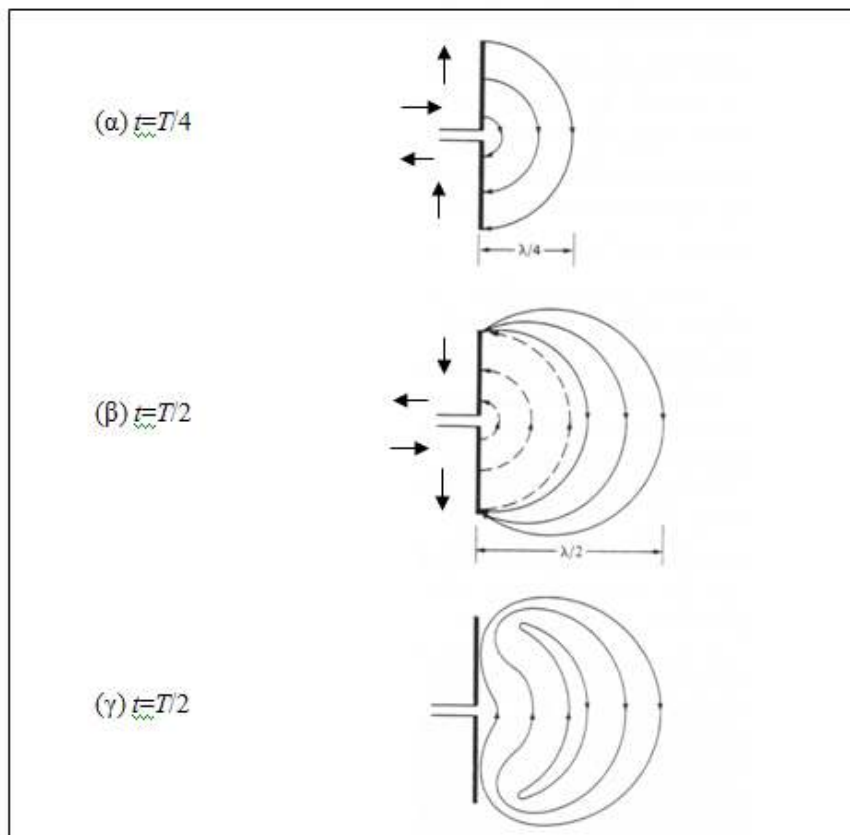


Figure 6.31: Concept of operation of an antenna device (Balanis, 2005).

More specifically, the antenna illustrated in Figure 6.30 above is a so-called *dipole antenna* and consists of two wires positioned in parallel on the same axis. The voltage or current coming from the generator through the transmission line creates a current flow on the antenna, and then electromagnetic waves are generated in free space due to the well-known Maxwell equations (Mitilineos, 2006).

The concept of operation of an antenna is further illustrated below using Figure 6.31 (Balanis, 2005). Consider a thin dipole antenna with a sinusoidal current flowing on its surface, i.e. a current of the form $I=I_0\sin(2\pi ft)=I_0\sin(2\pi t/T)$, I_0 being the amplitude, f being the frequency and T being the current's time period. The current flow direction on the antenna is indicated by arrows. During the first quarter time period, the electric field induced by the antenna to the nearby free space environment is indicated by the curves in Figure 6.31(a), covering a region of up to a quarter wavelength in distance. During the other quarter time period, newer electric field lines are introduced in the free space, while the previous ones have propagated another quarter wavelength in distance. Note that the direction of current and electric field is inverted during this time frame. Interestingly enough, at the time where $t=T/2$, the current on the antenna surface is equal to zero; thereupon, the electric field lines are detached from the antenna surface and configure closed loops, as indicated in Figure 6.31 (c).

The aforementioned procedure is repeated infinitely for as long as there is a current flowing in the antenna. Electric field lines are propagating further and further away from the antenna, reaching distant targets or other antennas acting as receivers.

The specifics of antenna theory and the respective equations and analysis comprise a scientific field with extreme breadth and depth, and will not be analyzed here for the sake of brevity and readability. The interested reader is referred to the referential work of C.A. Balanis, where a complete list of further literature can also be found (Balanis, 2005). Furthermore, the concept of smart antennas has been recently introduced in order to describe antennas that dynamically adapt to environmental conditions. This offers adaptive radiation patterns and input impedance, as well as a series of other specifications and applications, such as the estimation of the direction-of-arrival of the incoming signal; the aid in developing multiple-access information schemes; the advancement of the channel capacity; and others. Smart antennas consist of a number of simple antenna elements, that when combined with a smart processing circuitry, configure the smart antenna system. Further literature on the field can be found in (Mitilineos, 2006). In the following, a brief introduction to the main terminology and concepts of antennas and antenna arrays is cited in order to aid the interested reader in familiarizing with antenna fundamentals, including radiation patterns, gain and directivity, bandwidth and polarization.

6.5.2 Antenna radiation patterns

Perhaps the most important characteristic of an antenna is the way it converts the power delivered from the generator to electromagnetic waves propagated to various directions in space. The *antenna radiation pattern* is defined as “a mathematical function or a graphical representation of the radiation properties of the antenna as a function of space coordinates. In most cases, the radiation pattern is determined in the far-field region and is represented as a function of the directional coordinates. Radiation properties include power flux density, radiation intensity, field strength, directivity, phase or polarization” (Balanis, 2005). Often, field and power patterns are normalized with respect to their maximum value, yielding normalized patterns.

Regardless the specific antenna type, the radiated power attenuates inversely proportional to the square distance to the transmitter. Thereupon, antenna radiation characteristics may be summed up to the way a specific antenna radiates towards directions in space, (θ, ϕ) . In this sense, a radiation pattern may be calculated using (all of the following correspond to a closed curve or surface at a distance R):

- the received power $W_r(\theta, \phi)$ (Watt)
- the Poynting vector, P_{av} (Watt/m²)
- the radiation intensity $U(\theta, \phi) = R^2 P_{av}$ (Watt/sr)
- The respective normalized patterns may be calculated as in the following:

$$P(\theta, \phi) = \frac{W_r(R, \theta, \phi)}{W_r(R, \theta, \phi)_{\max}} = \frac{P_{av}(R, \theta, \phi)}{P_{av}(R, \theta, \phi)_{\max}} = \frac{U(\theta, \phi)}{U(\theta, \phi)_{\max}}, \tag{6.5.1}$$

where “max” figures correspond to maximum values regardless the angle (θ, ϕ) where they are observed.

Need help with your dissertation?

Get in-depth feedback & advice from experts in your topic area. Find out what you can do to improve the quality of your dissertation!

Get Help Now



Go to www.helpmyassignment.co.uk for more info



Radiation patterns are three dimensional; nevertheless, it is very common to use only one or two two-dimensional patterns over a predefined closed line at a distance R , e.g. for constant θ or constant φ . The most widely used 2D patterns are the ones referring to the so-called E - and H - planes (principal patterns). Figure 6.32 displays some of the most interesting antenna characteristics related to radiation patterns:

- **radiation lobes** are included between directions of minimum radiation. Lobes are designated as Main lobe, side lobes and back lobe. The main lobe includes the maximum radiated power direction. All other lobes are designated as “side lobes”, while the back lobe radiates towards the opposite direction with respect to the main lobe.
- the half-power or 3-dB radiation points, correspond to the angles where the radiated power is exactly the half with respect to the maximum one. The aperture between the left and right 3-dB points is called the 3-dB beamwidth.
- Null points are angles at which the radiation is minimized (not necessarily dropping to zero).
- Side-lobe level is the ratio of power radiated from side lobes with respect to the power radiated from the main lobe.

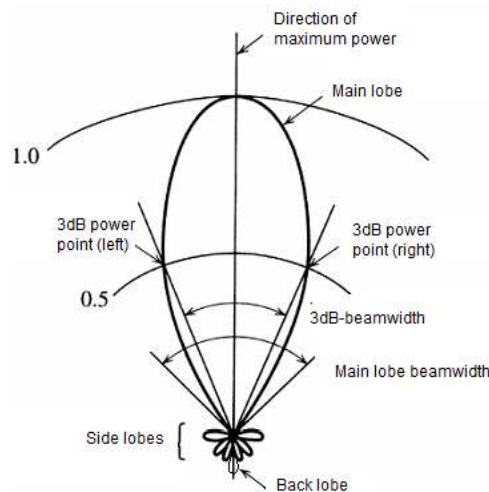


Figure 6.32: Normalized polar power pattern (S.P. Savvaidis, 2011).

In order to better understand the aforementioned terminology, consider an example of an antenna with a gain equal to 100, or equivalently 20dBi (see sub-section 5.1.2 for a definition of antenna gain). What does it take to read on such an antenna’s radiation pattern? In the following we take a closer look to the most commonly used pattern types, namely the polar, the dB-, and the Cartesian patterns.

6.5.2.1 Polar radiation pattern

Figure 6.34 displays an example of a polar *power* radiation pattern. The specific antenna has a direction of maximum directivity towards 22.5°. For any given angle, φ , the normalized value of the gain is equal to the distance between the origin of the coordinates system and the respective point on the pattern. E.g., for Figure 6.34 and an angle equal to φ the normalized gain is equal to 0.8. Given a gain of 100, it is concluded that the gain at angle φ is equal to 80.

Furthermore, the 3dB-beamwidth is graphically calculated using the directions at which the respective length equals 0.5. For the specific figure, the 3dB-beamwidth is designated as $\Delta 3dB$.

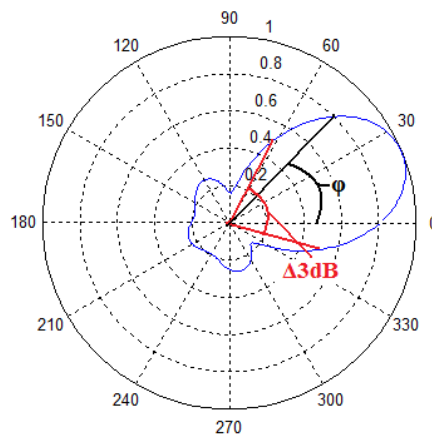


Figure 6.33: Polar radiation pattern example (S.P. Savvaïdis, 2011).

6.5.2.2 Polar radiation pattern in dB

Figure 6.34 displays an example of a polar *power* radiation pattern in dB.

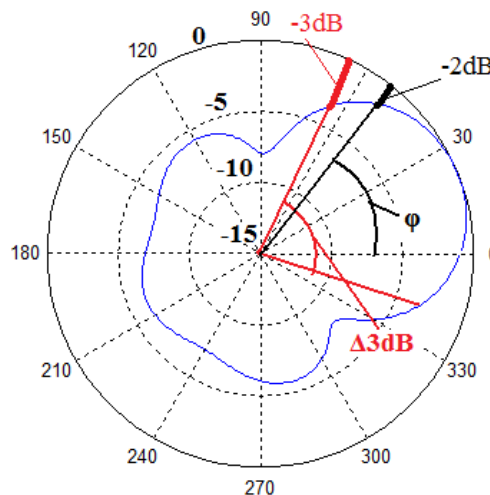


Figure 6.34: Radiation pattern of Figure 6.33, transformed in dBi (S.P. Savvaïdis, 2011).

In contrast to Figure 6.33, the above figure is characterized by that:

The minimum gain value in dB is defined by the user, and in this example is equal to -15dB (most inner circle in figure). Evidently, the gain value of -15dB is selected so as no direction corresponds to a smaller gain.

A normalized polar pattern range of values is between 0 and 1. Correspondingly, the values of the pattern in dB range between $-\infty$ and 0, respectively.

- The pattern in dB seems to be somewhat more stretched out with respect to the natural pattern.

Finally, in contrast to the previous procedure, the gain value at a given angle is calculated using the distance towards the most outer circle. E.g. for the angle φ in the figure, the distance towards the most outer circle is -2dB, thereupon the normalized gain at this angle is equal to -2dBi. Given the maximum gain to be equal to 20dBi, it turns out that the gain at this angle is equal to $20\text{dBi} - 2\text{dB} = 18\text{dBi} = 63.1$.

Brain power

By 2020, wind could provide one-tenth of our planet's electricity needs. Already today, SKF's innovative know-how is crucial to running a large proportion of the world's wind turbines.

Up to 25 % of the generating costs relate to maintenance. These can be reduced dramatically thanks to our systems for on-line condition monitoring and automatic lubrication. We help make it more economical to create cleaner, cheaper energy out of thin air.

By sharing our experience, expertise, and creativity, industries can boost performance beyond expectations. Therefore we need the best employees who can meet this challenge!

The Power of Knowledge Engineering

Plug into The Power of Knowledge Engineering.
Visit us at www.skf.com/knowledge

SKF



6.5.2.3 Cartesian radiation pattern in dB

Figure 6.35 displays an example of a cartesian *power* radiation pattern.

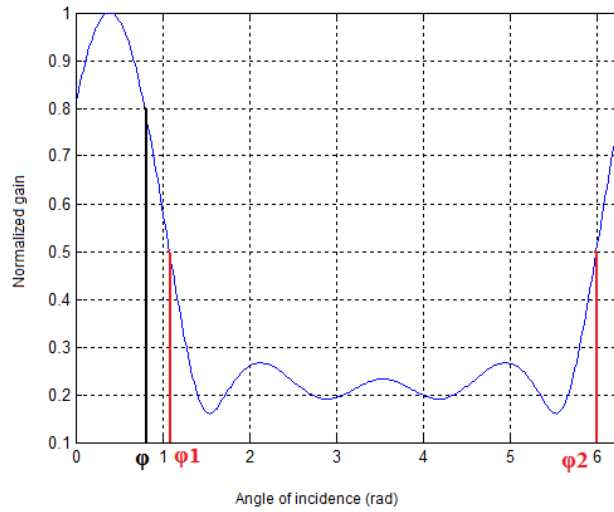


Figure 6.35: Radiation pattern of Figure 6.34 in Cartesian coordinates (S.A. Savvaidis, 2011).

The Cartesian pattern is the easiest to read, but the least used in practice nevertheless. Its use is straightforward, with every angle corresponding to a normalized gain indicated on the vertical axis, as in Fi.

6.5.3 Antenna gain and directivity

The *Antenna Gain* is a characteristic figure of antennas that corresponds to the antenna’s capability of aiming a narrow solid angle, or, similarly, of an antenna’s capability of collecting electromagnetic waves from narrow solid angles. The higher the antenna gain, the larger the current induced to a receiving antenna for a given distance and angles of transmission and reception. Moreover, it is empirically proven that the higher the antenna gain, the narrower the 3dB-beamwidth, and vice versa.

The isotropic radiator is used as a reference antenna in order to define gain. The isotropic radiator does not exist in nature but is rather a conceptual definition; it is supposed to be a radiator that radiates uniformly towards all directions, and its radiation pattern is a sphere. Furthermore, it is noted that since the gain of an antenna is compared to that of an isotropic radiation, the notation used in dB dictates that the antenna gain is given in dBi, “i” standing for “over isotropical”.

The gain of the isotropic radiator is defined to be unity, i.e. equal to 1. The gain of any antenna towards a given direction, (θ, ϕ) , corresponds to the ratio of the Poynting vector of the field generated by the antenna at a distance R , versus the Poynting vector of the field that would have been generated by the isotropic radiator at the same distance and with the same input power. Given that the isotropic radiator's gain is unity, the latter is calculated to be equal to $W_{in} / 4\pi R^2$. Thereupon, the antenna gain at any given angle (θ, ϕ) is given by

$$g(\theta, \phi) = \frac{P_{av}(\theta, \phi)}{W_{in} / 4\pi R^2} = \frac{4\pi R^2 P_{av}(\theta, \phi)}{W_{in}} = \frac{4\pi R^2 P_{av}(\theta, \phi)}{W_{rad} + W_{loss}}, \quad (5.2)$$

where W_{in} corresponds to the power that **enters the antenna** (not the power that is incident to the antenna, since a fraction of the latter is reflected back to the source; neither the power transmitted by the antenna, W_{rad} , since part of W_{in} is dissipated by the antenna producing mostly heat that is represented by W_{loss}).

It is usually implied that the “gain” corresponds to the maximum gain, regardless the direction where it appears. Thereupon, the “gain” in most textbooks is defined by

$$G = g(\theta, \phi)_{\max} = \frac{4\pi R^2 P_{av}(\theta, \phi)_{\max}}{W_{in}}. \quad (6.5.3)$$

In order to discriminate W_{in} to W_{rad} , **directivity** is defined similarly to gain, but now the calculations are referenced back to the radiated rather than the fed power, i.e.

$$d(\theta, \phi) = \frac{P_{av}(\theta, \phi)}{W_{rad} / 4\pi R^2} = \frac{4\pi R^2 P_{av}(\theta, \phi)}{W_{rad}}, \quad (6.5.4)$$

and, again, directivity is usually described as the maximum directivity, i.e. $D = d(\theta, \phi)_{\max}$.

Moreover, the **efficiency** of an antenna is defined as

$$n = \frac{W_{rad}}{W_{rad} + W_{loss}} = \frac{G}{D}. \quad (6.5.5)$$

Finally, another metric of gain or directivity is indirectly given by the **effective area** of an antenna that is defined by $a_e(\theta, \phi) = \frac{W_r}{P_{av}(\theta, \phi)}$, while, similarly as above, $A_e = a_e(\theta, \phi)_{\max}$. It is given that $A_e = \frac{\lambda^2}{4\pi} G$.

6.5.4 Antenna bandwidth

Antenna bandwidth is usually defined in terms of the respective reflection coefficient's bandwidth. More specifically, an antenna may be considered as a load connected to a transmission line. Following the analysis of earlier sections on transmission lines, the antenna bandwidth is usually defined as equivalent to the corresponding reflection coefficient's bandwidth. And, the reflection coefficient's bandwidth is defined as the frequency range within which the coefficient's amplitude remains within the limit of at most 3dB larger than its minimum value. A more loose but certainly most popular definition of bandwidth that is more usually used by field and development engineers is one that uses a maximum value of the reflection coefficient's value. E.g., the most widespread corresponding value is -10dB, which means that the bandwidth of the antenna is defined as the frequency range within which the reflection coefficient's amplitude is smaller than -10dB.

Another definition of antenna's bandwidth relates to the antenna's gain or directivity, and states that the antenna's bandwidth is the frequency range within which the gain remains within the limit of at most 3dB smaller than its maximum value.

Finally, a definition of antenna bandwidth that is unique for this class of devices is one that relates to the antenna's radiation pattern. More specifically, the antenna bandwidth may be defined as the frequency range within which the antenna's 3dB-beamwidth remains within certain limits with respect to its value at the central frequency (e.g. not varying more than 10%).



"I studied English for 16 years but...
...I finally learned to speak it in just six lessons"
Jane, Chinese architect

ENGLISH OUT THERE

Click to hear me talking before and after my unique course download



6.5.5 Antenna polarization

Finally, antenna polarization is defined according to the direction of the propagated electric field vector with respect to the horizontal plane (x-y plane, or ground plane) or a plane that is characteristic to the specific antenna type (e.g. dipole axis, larger side of a horn antenna, etc.). In this sense the terms horizontal or parallel, and vertical or perpendicular are used.

More specifically, if the lines of force of the electric field are in right angles with respect to the Earth's surface, then the wave is vertically polarized, whereas if the lines of force are parallel to the Earth's surface then the wave is horizontally polarized. For any other reference surface different to Earth, the respective definitions are "perpendicular" and "parallel" polarization respectively.

At times, the electric field's lines of force are neither horizontal neither vertical, nevertheless do have a constant direction; this is a linear polarization. Nevertheless, it is very usual that electric lines of force rotate; in such cases there may exist either the circular or elliptical polarization schemes, which are not further discussed herein.

6.5.6 Microstrip patch antennas

As long as textile antennas are concerned, it can be easily figured out that there are certain limitations on the available designs due to inherent limitations of the material on which such antennas are crafted (i.e. textile material). More specifically, due to the fact that textile antennas are actually intended to be used as *wearable* antennas, it happens that all the available designs and constructs in the literature refer to **textile patch antennas**. Thereupon, a short discussion on patch antennas is given below.

Microstrip patch antennas were first introduced during the second half of the twentieth century and are based on the observance that microstrips may radiate electromagnetic waves effectively given certain limitations (Mitropoulos, 2005). An example of a patch antenna is depicted in Figure 6.36. In the left side of the figure, the width and length of the patch are illustrated, together with the feeding transmission line (the line is connected to the source). Also, there is a substrate of thickness h , and a ground plane. The substrate has a relative permittivity equal to ϵ_r , while the thickness of the patch is equal to t .

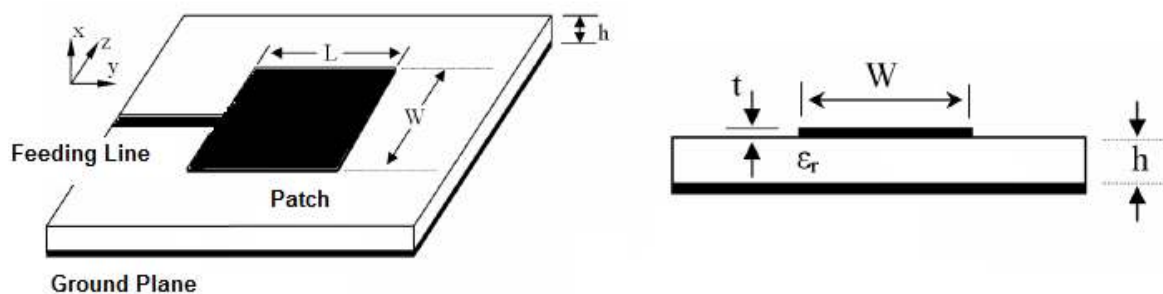


Figure 6.36: Patch antenna design example (Angle and side views).

Due to inherent design limitations, patch antennas usually radiate most effectively towards the direction that is perpendicular to the substrate surface and opposite to the ground plane. Different patch layouts are proposed in the literature, yielding rectangular, circular, ring, or other complex patch layouts. More specifically, there are analytic expressions yielding the appropriate width and length of a rectangular patch like the one in Figure 6.36 according to the desired frequency of operation; nevertheless the simple shape of the patch in Figure 6.36 results in a narrow bandwidth and linear polarization. In order to achieve circular or other polarization schemes, various patch shapes are introduced, like the circular ring patch in Figure 6.37(a). Other shapes that are more appropriate in order to achieve higher bandwidths include asymmetric patch corners and metal cut-outs at the point where the transmission line enters the patch, like in Figure 6.37(b).

Furthermore, a patch antenna may be fed using a microstrip or coaxial probes (see), or even using sophisticated techniques of induced fields due to proximity to nearby transmission lines etc. (Balanis, 2005) (Mitropoulos, 2005). Feeding a patch antenna also plays an important role on the achieved polarization, i.e. asymmetric feeding may result to circular or other polarization according to design requirements.

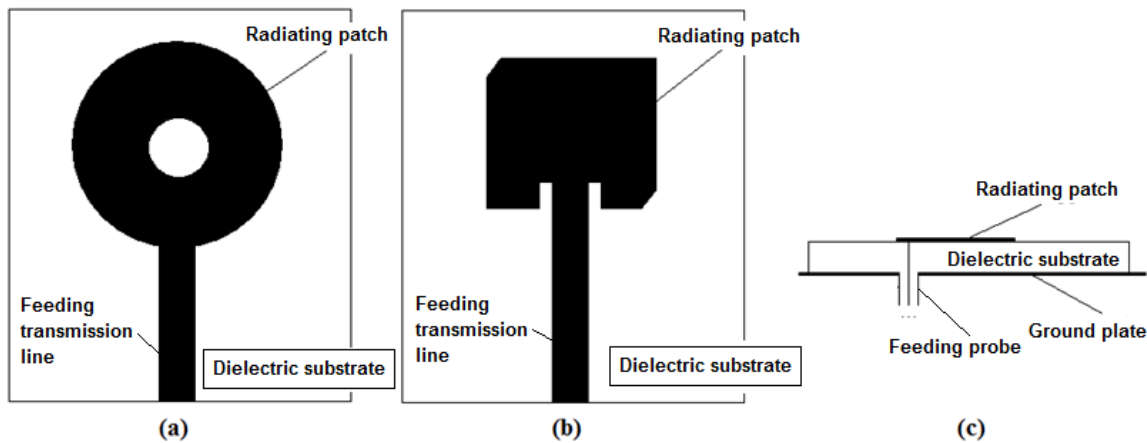


Figure 6.37: Various patch shapes and feeding techniques.

The length and width of a patch usually range between $\lambda/2$ and $3\lambda/2$, while the relative permittivity ranges between 2 and 12. Large thickness values and lower permittivity values are in general more efficient, in that they yield larger bandwidth and efficiency antennas (Mitropoulos, 2005). In the following Section, a more detailed discussion on textile patch antennas is given.

6.6 Textile antennas

6.6.1 Textile antennas in the literature

Research and technology development on textile antennas followed the introduction of the smart textiles concept in the nineties. Smart textiles are a generic term implying textiles with advanced functionality (mainly with respect to certain electrical-related characteristics) that can be applied to any industry from home to automotive and industrial applications; on the other hand, wearable smart textiles and thereby wearable sensors, antennas, chips etc. correspond to a specific applications area related to clothing and clothing materials. In recent years there has been an extensive research activity on the field of wearable computing, with passive and active components sewn on fabric and offering the means for developing wearable communications modules.

The main idea behind this concept is that smart textiles may be used as a platform carrying smart sensory and actuator systems, mainly for developing applications around a person or groups of persons. Smart wearable textiles are being made available today due to the availability of micro-electronics on the one hand and of new textile materials on the other, and according to Hertleer are classified as passive, active, and smart textiles. Passive textiles host sensors that collect data regarding biological, environmental and other data, active textiles may on top of passive actuate external switches and functions, and smart textiles may adapt their behavior according to the environmental and other circumstances (Hertleer C. , 2009). One particular area of research on the field is the design and development of antennas and antenna arrays on conductive fabric surfaces (textile antennas), i.e. using the cloth itself as the communication module rather than as a module host.

What do you want to do?

No matter what you want out of your future career, an employer with a broad range of operations in a load of countries will always be the ticket. Working within the Volvo Group means more than 100,000 friends and colleagues in more than 185 countries all over the world. We offer graduates great career opportunities – check out the Career section at our web site www.volvogroup.com. We look forward to getting to know you!

VOLVO
AB Volvo (publ)
www.volvogroup.com

VOLVO TRUCKS | RENAULT TRUCKS | MACK TRUCKS | VOLVO BUSES | VOLVO CONSTRUCTION EQUIPMENT | VOLVO PENTA | VOLVO AERO | VOLVO IT
VOLVO FINANCIAL SERVICES | VOLVO 3P | VOLVO POWERTRAIN | VOLVO PARTS | VOLVO TECHNOLOGY | VOLVO LOGISTICS | BUSINESS AREA ASIA



A wearable textile system will ideally comprise several components, like sensors, actuators, processing units, energy supplies, and a communication system. Ongoing research aims at developing circuit components and, eventually, integrated data processing and communication units out of clothing material. Up to day and to the best of our knowledge, only sensors and antennas have been successfully implemented using solely textile materials. Moreover, out of all the available design approaches, planar patch antennas are the most suitable, when using textile materials for antenna development, since they allow an easy integration with conventional clothing. Thereupon, textile antennas available in the literature currently solely employ planar patch designs.

It is widely considered that the development of textile antennas will be greatly beneficial to end-users like civil protection units, first responders etc., elderly users or patients in hospitals, or even everyday users for widespread commercial applications and smart networking. Indeed, textile antennas will greatly leverage performance and comfort of smart textile systems, by offering higher gain and operability with respect to integrated antennas while at the same time offering comfort and ease of use with respect to external but rigid antennas.

The feasibility of higher-than-normal antennas is also legitimate, mainly due to the large area of deployment that is available on the cloth surface giving the designer many choices and large margins from an antenna design point of view. Actually, the available area on a cloth's surface allows possibilities like using co-planar structures and/or planar arrays with antenna elements that may be selected from a wider set of different antenna types, as well as employment of different diversity schemes. However, the wearable character of the antenna obliges the designer to also examine the physical and physiological properties of the end product in order to avoid comfort problems which would potentially limit the success of the wearable textile based antennas.

Research and technology development regarding textile antennas can be traced back to the beginning of the new millennium, when wearable antennas partially based on textiles, were presented by Salonen et al. (P. Salonen, 2004). In particular, Salonen et al. dealt with the match performance and radiation characteristics of the antenna, as well as with the power absorbed by the human body. In consequent publications, Salonen et al. presented a dual-band E-shaped patch textile antenna, as well as specific studies on the behavior of an antenna under certain circumstances like bending etc. Furthermore, hybrid antennas using both metallic parts and fabrics were presented by Klemm, Santas and Nurul (M. Klemm, 2006), (J.G. Santas, 2007) and (H.M.R. Nurul, 2010).

On the other hand, pure textile microstrip antennas have been investigated for employment in various frequency bands. Hertleer et al., as well as Vallozzi et al. reported 2.4GHz antennas for fire fighter garments that are made purely of textile-material (Hertleer, 2009) (L. Vallozzi, 2010). Santas et al. introduced a textile antenna for UHF-VHF bands (J.G. Santas, 2007b), while discussed the effects of variations in material property on a textile antenna performance. Dierck et al. proposed a textile patch antenna suitable for the GPS L1 band at 1.57542GHz in (A. Dierck, 2010). Furthermore, Alomainy et al. provided a parametric study of wearable antennas on various distances from the body (A. Alomainy, 2007). Distance from the bearer's body may have a substantial effect on an antenna's performance; backwards radiation may be suppressed using ground planes, but then additional elements need to be used in order to cover the entire azimuth plane. Dual-band textile antennas have also been reported, like an antenna for the 2.4GHz and 5GHz bands on EBG substrate by Zhu and Langley (S. Zhu, 2009) The effect of bending and crumpling has been also investigated by Bai and Langley that made an extensive study on the effects that bending may have on an antenna's efficiency, radiation pattern, gain and matching (Q. Bai, 2009).

Other research results towards the development of textile antennas include certain research projects, like an undergoing ESA project aiming at developing textile antennas for Iridium operating frequencies that require antennas with circular polarization. Furthermore, the European project ProeTex aims at developing smart electro-textile garments for firefighters and first responders at security missions (<http://www.proetex.org/>). The SFIT cluster is a European initiative and comprises a cluster of EU funded research projects, aiming to bring together projects addressing the area of Smart Fabrics, Interactive Textile (SFIT) and flexible wearable systems (<http://csnej106.csem.ch/sfit/>). Furthermore, SYSTEX is a coordination and support action project aiming at enhancing the research on wearable microsystems and e-textiles (<http://www.systex.org>).

Evidently, textile antennas despite comprising a relatively new technology have already come up with certain design and development examples, in several frequency bands, while various issues have been studied or confronted, like bending, textile substrate electrical characteristics robustness, dual band and wide band operation etc. Nevertheless, textile antennas are still an immature technology, and there are certain issues of particular interest that an interested designer needs to take into account, on top of concerns related to classical antenna design and development.

First of all, it is still unclear what are the electrical characteristics and properties of woven, knitted, sewn or embroidered conductive and dielectric fabrics. It is important to test and evaluate market-available conductive fabrics of various types, with respect to their electrical characteristics and their eligibility to be used as a basis for antenna development, as well as with respect to their properties as clothing materials. Specific and detailed models are needed, since the aforementioned characteristics are subject to change with respect to fabric density, waving techniques used, moisture absorbed by the fabric etc. Then, an antenna design should be tested in simulation regarding its behaviour under various bending and crumpled conditions, as well as change of electrical characteristics due to moisture and sweat absorption by the material.

Furthermore, conductive fabrics should possess a low and stable electrical resistance in order to suppress non-radiative losses i.e. Ohmic or reactive losses. A fabric with a resistance less than 1 Ohm/sq.m is considered as a rough limit for feasible operation (I. Locher, 2006). Furthermore, the fabric should be flexible enough to provide wearing comfort while at the same time the mechanical properties should allow a reasonably low degree of deformation of the antenna shape and, consequently, of its radiation properties. On the other hand, dielectric fabrics may be used as a substrate material. Electrical permittivity and permeability of the dielectric fabric should be carefully measured and apparently the dielectric fabric should exhibit the lowest possible conducting losses, i.e. a low loss tangent, in order to increase the antenna's efficiency. Furthermore, low permittivity is desired since it generally provides better efficiency and better bandwidth (Balanis, 2005) (I. Locher, 2006). Finally, a thickness of a few millimetres is desired, whereas the anticipated thickness variation of typical clothing materials should be kept as low as possible.

gaiteye[®]
Challenge the way we run

**EXPERIENCE THE POWER OF
FULL ENGAGEMENT...**

**RUN FASTER.
RUN LONGER..
RUN EASIER...**

**READ MORE & PRE-ORDER TODAY
WWW.GAITEYE.COM**

Besides the electric properties of the conductive and dielectric fabrics, additional fabric properties – depending on the role of the fabric and its contribution in the final garment's structure – must be taken into account: a) Mechanical properties (Tensile, tearing, etc.) b) Comfort properties (hand evaluation, thermal properties, water vapour permeability, etc.), c) Appearance properties (colour stability, shrinkage, etc.). The final design and fabrication decisions should consider implementation parameters in the garment, making sure that it will conform to rules of industrial scale production and ensuring that multifunctional garments will be available under feasible cost conditions and in adequate quantities.

6.6.2 Numerical and measurements results

In order to demonstrate the feasibility and applicability of textile antennas design and development, two test cases are presented herein that can be found in the literature. The first is a rectangular-ring shaped antenna for firefighter garment introduced by Hertleer et al. (Hertleer C.V.-L., 2007), and the second is a linear polarization patch antenna on felt substrate for 2.4 GHz communications introduced by Locher et al. (I. Locher, 2006).

6.6.2.1 A rectangular-ring shaped antenna for firefighter garment (Hertleer C.V.-L., 2007)

In this work, Hertleer et al. presented a textile antenna developed on aramid fabric with the purpose of integrating it on a firefighter's garment for short range communication to transmit the fire fighter's life signs to a nearby base station. The antenna's shape was that of a rectangular ring (see Figure) and it was optimized for operation within the entire 2.4-2.4835 GHz frequency band. More specifically, a bandwidth of return loss lower than -10dB was required, while the antenna gain should be maximized for the aforementioned frequency band.

The proposed antenna in realistic operational conditions was supposed to be covered with several layers of textile material (comprising the protective garment of the firefighter) that would affect the antenna's characteristics. Furthermore, the antenna should operate in the presence of a body, which further affects the antenna. According the Hertleer, the proposed antenna provides enough robustness to preserve its characteristics under these circumstances.

Reproduction and Original Electrical Characteristics		Reproduction Results		Original Results
Substrate thickness	1.73 mm	Gain	3.6 dBi	Gain
Ground plane	10cm x 10cm	-10dB return loss bandwidth	125 MHz	-10dB return loss bandwidth
ϵ_r	1.85	3-dB beamwidth	66°	3-dB beamwidth
$\tan \delta$	0.015			

Table 6.2: Electrical characteristics and results comparison between reproduction and the antenna reported in (Hertleer C.V.-L., 2007).

In order to verify Hertleer's allegation, we reproduced the proposed antenna in a commercially available simulator and extracted numerical results regarding its return loss and gain radiation pattern. Herein, by "reproduced" we mean that we extracted the patch dimensions and electrical characteristics, designed a similar patch in the simulator and analyzed the proposed antenna in order to get the numerical results that are presented herein.

The dimensions and electrical characteristics of the reproduction were based on data included in the work of Hertleer. The former are illustrated in Figure 6.38 (upper left), while the latter are included in Table 6.2. According to our results, the antenna gain is equal to 3.6 dBi at boresight, with a 3-dB beamwidth equal to 66° and a -10dB return loss bandwidth equal to 125 MHz (the band 2.4-2.4835 GHz included). The corresponding results of the original antenna were reported as in the following: gain equal to 4.36 dBi and 3.83 dBi (antenna uncovered or covered with protective garment respectively), -10dB return loss bandwidth slightly over 100 MHz, and 3-dB beamwidth equal to 71.1° and 70.2° (uncovered and covered respectively). Furthermore, the antenna gain measured in proximity to a human body was found to be equal to 3 dBi. According to the above, it is concluded that (i) the reproduced antenna's radiation characteristics are similar to the ones reported for the measured prototype and (ii) the proposed antenna is suitable for 2.4 GHz ISM band applications.

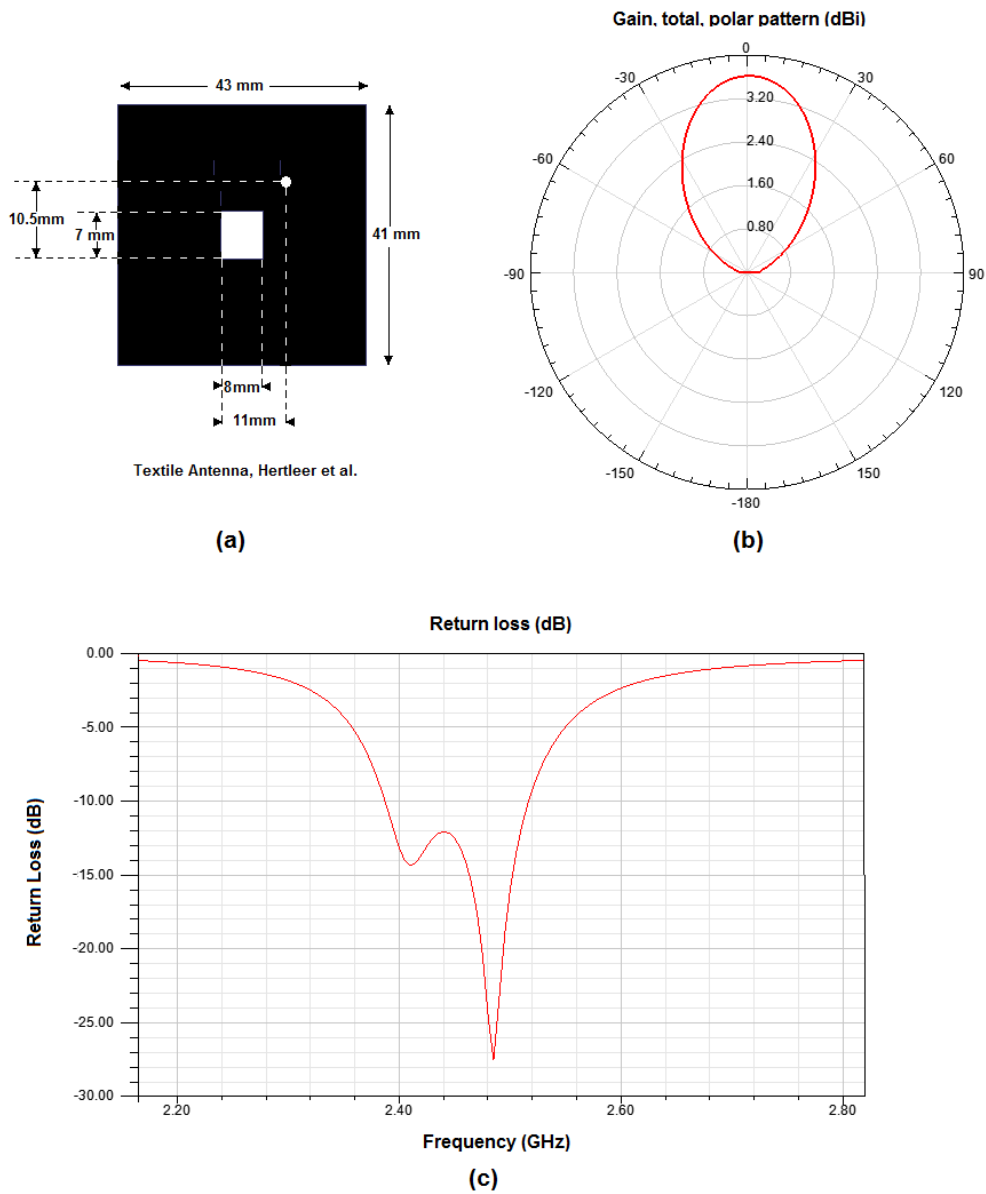


Figure 6.38: Reproduction and simulation results of a textile antenna for firefighter garments at 2.45 GHz (Hertleer C. V.-L., 2007).

6.6.2.2 A linear polarization patch antenna on felt substrate for 2.4 GHz communications (I. Locher, 2006)

In this work, Locher et al. presented a detailed study on the design and characterization of purely textile patch antennas, including characterization of the electrical properties of several substrate materials available for the development of textile antennas. In this context, four textile antennas are presented, based on various substrates and with different polarizations. All antennas are fed via a microstrip line and are designed to operate in the 2.4 GHz ISM band. According to the authors, a microstrip feed not only guarantees a flat structure, but also allows the assembly of electronic components directly on the fabric in antenna proximity.

Out of the four antennas presented in this work two of them are circularly polarized, and two of them are linearly polarized. Furthermore, two of them are developed over a felt substrate with a thickness of 3.5 mm, and two of them are developed over a spacer substrate with a thickness of 6 mm. For comparison purposes, we have reproduced the linear polarized antenna over a felt substrate, using a commercially available simulator, and numerical results are presented herein.

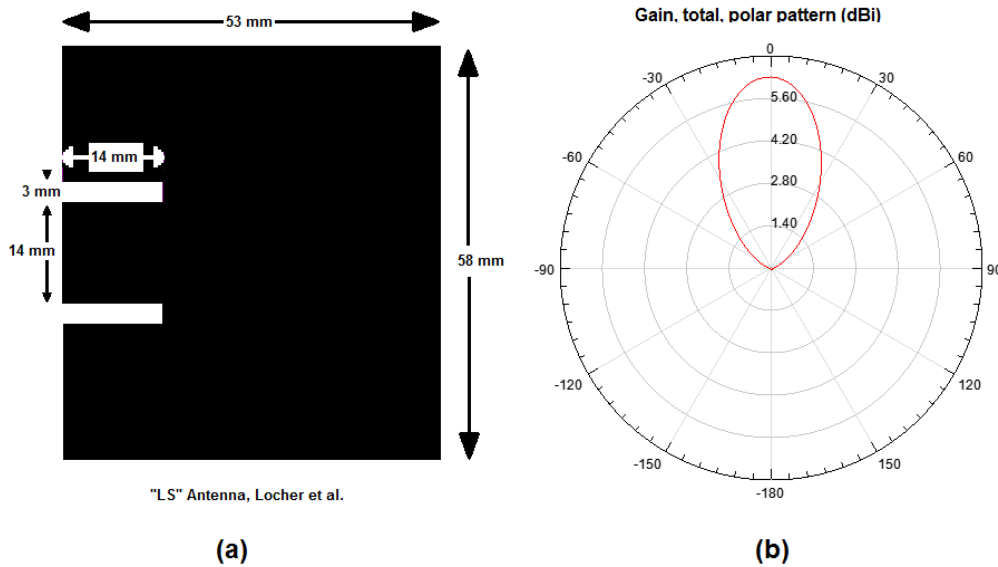


Figure 6.39: Reproduction and simulation results of a textile antenna with felt substrate and linear polarization at 2.4 GHz (I. Locher, 2006).

Reproduction and Original Electrical Characteristics		Reproduction Results		Original Results
Substrate thickness	3.5 mm	Gain	6.3 dBi	Gain
ϵ_r	1.45	3-dB beamwidth	58°	3-dB beamwidth
$\tan \delta$	0.02			

Table 6.3 : Electrical characteristics and results comparison between reproduction and the antenna reported in (I. Locher, 2006).

In order to verify Locher’s design, we reproduced the linear polarized antenna case over a woolen felt substrate and extracted numerical results regarding its return loss and gain radiation pattern. Again, by “reproduced” we mean that we extracted the patch dimensions and electrical characteristics, designed a similar patch in the simulator and analyzed the proposed antenna in order to get numerical results.

The dimensions and shape of the antenna are illustrated in Figure 6.40 (left), while the electrical characteristics of the patch and substrate are tabulated in table 6.3 above, together with numerical and compared measurements results. According to our results, the antenna gain is equal to 6.3 dBi at boresight, with a 3-dB beamwidth equal to 58°. Correspondingly, the original antenna was measured with a gain of 5.5 dBi in the case where a conductive fabric was used, and 9.0 dBi in the case where a copper foil was used, while the 3-dB beamwidth when using the conductive fabric was measured equal to 57° and 78° under flat and bent conditions respectively. Again, it is concluded that the reproduced antenna's radiation characteristics are similar to the ones reported for the measured prototype, while at the same time the proposed antenna is suitable for 2.4 GHz ISM band applications.

6.7 References

(A. Alomainy, 2007) Alomainy, A., Yang, H., and Davenport, D.M., "Parametric study of wearable antennas with varying distances from the body and different on-body positions", *IET Seminar on antennas & propagation for body-centric wireless communications*, London, April, 24, 2007.

(Q. Bai, 2009) Bai, Q., and Langley, R., "Crumpled textile antennas", *Electronics Letters*, Vol. 45, p. 436, 2009.

(Balanis, 2005) C.A. Balanis, *Antenna Theory: Analysis and Design*, John Wiley & Sons, Hoboken, New Jersey, USA, 2005.

(D. Cottet, 2003) D. Cottet, J. Grzyb, T. Kirstein and G. Troster, "Electrical characterization of textile transmission lines", *IEEE Transactions on Advanced Packaging*, Vol. 26, No 2, 182–189, (2003).

(Y.-H. Chou, 2008) Y.-H. Chou, M.-J. Jeng, Y.-H. Lee and Y.-G. Jan, "Measurement of RF PCB dielectric properties and losses", *PIER Letters*, Vol. 4, 139–148, (2008).

(A. Dierck, 2010) Dierck, A., De Keulenaer, T., Declercq, F., and Rogier, H., "A wearable active GPS antenna for application in smart textiles", *32nd ESA Antenna Workshop on Antennas for Space Applications*, pp. 1–4, Noordwijk, The Netherlands, October, 5–8, 2010.

(M. Dirix, 2012) M. Dirix, O. Koch 'Conductivity Measurements of Silverpastes' *Acta Polytechnica*, Vol. 50 No. 4 (2010).

(Hertleer, 2009) C. Hertleer, *Design of Planar Antennas Based on Textile Materials*, Ph.D. Dissertation, Ghent University, Belgium, 2009.

(Hertleer C.R., 2009) Hertleer, C., Rogier, H., Valozzi, L., and Van Langenhove, L., “A textile antenna for off-body communication integrated into protective clothing for firefighters”, *IEEE Transactions on Antennas and Propagation*, Vol. 57, No. 4, p. 919, April 2009.

(Hertleer C.T., 2008) Hertleer, C., Tronquo, A., Rogier, H., Van Langenhove, L., “The use of textile materials to design wearable microstrip patch antennas”, *Textile Research J.*, vol. 78, no. 8, pp. 651–658, Aug 2008.

(Hertleer C.V.-L., 2007) C. Hertleer, L. Van-Langenhove, H. Rogier, and L.A. Vallozzi, “A textile antenna for firefighter garments”, *Proceedings of AUTEX 2007*, Tampere, Finland, 26–28 June 2007.

(T.F. Kennedy, 2009) Kennedy, T.F., Fink, P.W., Chu, A.W., Champagne, N.J., Lin, G.Y. and Khayat, M.A., “Body-Worn E-Textile Antennas: The Good, the Low-Mass, and the Conformal”, *IEEE Transactions on Antennas and Propagation*, Vol. 57, No. 4, April 2009.

(M. Klemm, 2006) Klemm, M., Troester, G., “Textile UWB antennas for wireless body area networks”, *IEEE Transactions on Antennas and Propagation*, Vol. 54, No. 11, pp. 3192–3197, Nov 2006.

(I. Locher, 2006) I. Locher, M. Klemm, T. Kirstein, and G. Troster, “Design and characterization of purely textile patch antennas”, *IEEE Transactions on Advanced Packaging*, Vol. 29, No. 4, pp. 777–788, November 2006.



(J.C.G. Matthews, 2009) Matthews, J.C.G., Pettitt, G., “Development of Flexible, Wearable Antennas”. 3rd European Conference on Antennas and Propagation, Berlin, Germany, March, 23–27, 2009.

(Mitilineos, 2006) S.A. Mitilineos, *Multipath Fading Mitigation Using Smart Antennas*, PhD Dissertation, NTUA Press, Athens, Greece, 2006.

(Mitropoulos, 2005) G.K. Mitropoulos, *Development of Integrated Patch Phased Array on Variable Permittivity Substrates*, PhD Dissertation, NTUA Press, Athens, Greece, 2005.

(H.M.R. Nurul, 2010) Nurul, H.M.R., Malek, F.S., Vandenbosch, G.A.E., Volski, V., Ooi, S.L., and Adam, I., “Evaluation of a wearable hybrid textile antenna”, *Loughborough Antennas and Propagation Conference*, p. 337, Loughborough, UK, November, 8–9, 2010.

(Y.J. Ouyang a. W., 2007) Y. Ouyang, W. Chappell, “Measurement of electrotexiles for high frequency applications,” *Proc. IEEE MTT-S Int. Microwave Symposium*, pp.1679–1682, 2005.

(Y.J. Ouyang, 2008) Y. Ouyang, W.J. Chappell. “High frequency properties of electro-textiles for wearable antenna applications”, *IEEE Trans. Antennas and Prop.*, Vol. 56, No 2, 381–388 (2008).

(Pozar, 2005) D.M. Pozar, *Microwave engineering*, 3rd ed. Wiley, (2005).

(P.J. Soh, 2011) P.J. Soh, G.A.E. Vandenbosch, X. Chen, P.S. Kildal, S.L. Ooi, H. Alikbarian, “Wearable textile antennas’ efficiency characterization using reverberation chamber”, *IEEE, AP-S/URSI 2011*.

(P. Salonen, 2004) Salonen, P., Rahmat-Samii, Y., and Kivikoski, M., “Wearable antennas in the vicinity of human body”, *IEEE Antennas and Propagation Society Symposium*, June, 20–25, 2004.

(S. Sankaralingam, 2010) Sankaralingam, S., and Gupta, B., “Development of textile antennas for body wearable applications and investigations on their performance under bent conditions”, *Progress In Electromagnetic Research B*, Vol. 22, pp. 53–71, 2010.

(J.G. Santas, 2007) Santas, J.G., Alomainy, A., and Yang, H., “Textile antennas for on-body communications: techniques and properties”, *European Conference on Antennas and Propagation*, pp. 1–4, Edinburgh, UK, November, 11–16, 2007.

(S.P. Savvaïdis, 2011) S.A. Savvaïdis, and S.A. Mitilineos, *Antennas, Radio Propagation and Radar Laboratory Notes*, TEI of Piraeus, Athens, Greece, 2011.

(L. Vallozzi, 2010) Vallozzi, L., Van Torre, P., Hertleer, C., Rogier, H., Moeneclaey, M., and Verhaevert, J., “Wireless communication for firefighters using dual-polarized textile antennas integrated in their garment”, *IEEE Transactions on Antennas and Propagation*, Vol. 58, No. 4, pp. 1357–1368, April 2010.

(S. Vassiliadis, 2011) S. Vassiliadis, N. Stathopoulos, K. Prekas, S. Savaidis, “Behaviour of the conductive yarns and fabrics in high frequencies”, *ITMC 2011 International Conference, Casablanca, 2011*.

(S. Zhu, 2009) Zhu, S., and Langley, R., “Dual-band wearable textile antenna on an EBG substrate”, *IEEE Transactions on Antennas and Propagation*, Vol. 57, No. 4, pp. 926–935, 2009.